

Non-Markovian dynamics of a biased qubit coupled to a structured bath

Congjun Gan [‡], Peihao Huang, Hang Zheng

Department of Physics, Shanghai Jiao Tong University, Shanghai 200240, People's Republic of China

E-mail: gancongjun@sjtu.edu.cn

Abstract. A new analytical approach, beyond rotating wave approximation, based on unitary transformations and the non-Markovian master equation for the density operator, is applied to treat the biased spin boson model with a Lorentzian structured bath for arbitrary detunings at zero temperature. Compared to zero bias, we find that the dynamics demonstrates two more damping oscillation frequencies and one additional relaxation frequency for non-zero bias, where one of the damping oscillation frequencies is a new effect. Analytical expressions for the non-Markovian dynamics and the corresponding spectrum, the localized-delocalized transition point, the coherent-incoherent transition point, the analytical ground energy, the renormalized tunneling factor and the susceptibility are determined. The sum rule and the Shiba relation are checked in the coherent regime.

PACS numbers: 05.40.-a, 03.67.-a, 05.30.-d

Keywords: Spin boson model, Lorentzian bath, Non-Markovian

Submitted to: *J. Phys.: Condens. Matter*

1. Introduction

In a fully quantum-mechanical way, the spin boson model (SBM) [1, 2, 3] is a prominent physical model in the research of dynamics and decoherence for numerous physical and chemical processes. Due to its advantage in the quantitative description of quantum bit (qubit), the SBM has drawn wide interest in the quantum mechanics field. In the last decade, many promising scalable solid-state qubit schemes have been proposed and realized [4, 5, 6, 7]. Since controlling decoherence is the dominating strategy in solid-state qubit [8, 9], qubit can be designed to be coupled to a harmonic oscillator (HO) or detector instead of the dissipative environment in order to minimize the decoherence. The HO is coupled further to the environment [6, 7, 10, 11], which is usually characterized by an Ohmic spectral density $J_{\text{Ohm}}(\omega)$. Such a qubit-HO-environment proposal can be realized as: a flux-qubit read out by a dc-SQUID [6, 7, 12] or a qubit placed in a leaky cavity [6, 7, 11]. Since we usually only need to consider two primal states in the qubit and the environment is characterized by the Ohmic bath, as an alternative but equivalent point of view, such a qubit-HO-environment model can be exactly mapped to the SBM with a Lorentzian structured bath $J(\omega)$ (see (6) in Sec. 2) [13, 14, 15, 16].

Different from the Ohmic bath, the equilibrium dynamics of the SBM with such a structured bath or the equivalent qubit-HO-environment model is rarely studied in the papers, such as the studies on a driven qubit coupled to a structured environment by Grifoni et al. [17, 18]. However, this paper is interested in the regime with static bias and typical studies include the quasi-adiabatic propagator path integral (QUAPI) [19], the Van Vleck perturbation theory together with a Born-Markov master equation (VVBM) [20], the flow equation renormalization (FER) [21, 22, 23], the non-interacting blip approximation (NIBA) [22, 24], an approximation scheme by introducing a HO displacement operator [25] and the perturbation method based on unitary transformation [26]. It's known that QUAPI is mainly numerical and it is restricted to finite temperature [23]. VVBM works well with finite bias at low temperature and Ref. [20] is a nice and physically clear work. However, since VVBM uses the Van Vleck perturbation theory up to the second order in the qubit-HO coupling to get the eigenvalues and eigenfunctions of the non-dissipative qubit-HO system and solves a Born-Markov master equation for the reduced density matrix in the qubit-HO's eigenbasis, it requires a small qubit-HO coupling and a Born-Markov approximation [20]. To our knowledge, FER has not studied the non-equilibrium dynamics and it needs to choose extra setting parameters for its best results [27]. Until now, NIBA is not applicable for non-zero bias at low temperature [20, 22, 24]. Ref. [25] presents only results for zero bias near resonance, meanwhile, Ref. [26] with one unitary transformation only presents results for zero bias as well.

In this paper, as an extension to Huang and Zheng's work [26, 28], a new analytical approach, beyond rotating wave approximation (RWA), based on two unitary transformations and the non-Markovian master equation for the density operator, is

applied to treat the biased spin boson model (SBM) with a Lorentzian structured bath for arbitrary detunings at zero temperature. One should note that the two unitary transformations are different from Ref. [26, 28] and it makes our approach applicable both for non-zero bias and zero bias. Moreover, within a nontrivial Born approximation but without Markovian approximation, we get the analytical density operator by the master equation method, which can easily be extended to finite temperature comparing with Ref. [28]. Our approach has several advantages. First, both the localized-delocalized transition point α_L and the coherent-incoherent transition point α_c are studied, which have not been provided so far (except α_c with zero bias by Ref. [26]). Second, it works well for a wide parameter range: having no direct restriction on the qubit-HO coupling, both for biased and unbiased, at arbitrary finite detunings (positive/negative detunings or on resonance) and with sufficient strong spin-bath coupling as long as $\alpha < \alpha_c$, which is little-studied and beyond the weak coupling regime. Our results are checked in the exactly solvable special cases. The dynamics and the corresponding spectrum are compared to the literature results both for unbiased and biased cases. The Shiba relation and the sum rule have also been examined.

This paper is organized as follows. Sec. 2 introduces the model and our treatment. Meanwhile, the ground state energy, the renormalized tunneling factor η and localized-delocalized transition point α_L are determined. Sec. 3 presents the master equation and an analytical expression for the density operator without Markovian approximation. In Sec. 4, we have calculated the non-equilibrium dynamics $P(t)$ and the corresponding spectrum $S(\omega)$, and presented the physical interpretation. In Sec. 5, it shows the susceptibility and the validation of the Shiba relation. The coherent-incoherent transition point α_c is determined.

2. Model and treatment

In a flux qubit system, the qubit is the two macroscopically distinct quantum states representing clockwise and anticlockwise rotating supercurrents. The qubit is entangled with the detecting field, which is itself coupled with the outside noncoherent environment. The qubit can be characterized by Pauli matrices, the detecting equipment, which is actually a LC resonant circuit[6, 7], can be described by a harmonic oscillator with a characteristic frequency Ω and the environment can be described by a set of harmonic oscillators. Therefore, the qubit-HO-environment Hamiltonian can be written as (with Planck units $\hbar = k_B = 1$):

$$H = -\frac{\Delta}{2}\sigma_x + \frac{\epsilon}{2}\sigma_z + \Omega A^\dagger A + \sum_k \omega_k a^\dagger a + (A^\dagger + A) \left[g\sigma_z + \sum_k \kappa_k (a_k^\dagger + a_k) \right] + (A^\dagger + A)^2 \sum_k \frac{\kappa_k^2}{\omega_k}, \quad (1)$$

where Δ is the energy difference of the qubit and ϵ is the applied bias; A (or A^\dagger) and a_k (or a_k^\dagger) are the annihilation (or creation) operators of harmonic oscillators with

frequencies Ω and ω_k 's, respectively; g is the qubit-HO coupling and κ_k is the HO-environment coupling relating to the k th oscillator. The environment is described by the Ohmic spectral density as $J_{\text{Ohm}}(\omega) \equiv \sum_k \kappa_k^2 \delta(\omega - \omega_k) = \Gamma\omega$, where Γ is the dimensionless coupling constant to describe the Ohmic bath.

As an alternative but equivalent point of view, such a qubit-HO-environment model in (1) can be exactly mapped to the conventional SBM with a Lorentzian structured bath. The Hamiltonian reads [13, 14, 15, 16, 26]

$$H = H_S + H_B + H_I, \quad (2)$$

where the subscript 'S' denotes the spin system, the subscript 'B' denotes the boson environment and the subscript 'I' denotes the interaction between the spin and the boson environment, with

$$H_S = -\frac{\Delta}{2}\sigma_x + \frac{\epsilon}{2}\sigma_z, \quad (3)$$

$$H_B = \sum_k \omega_k b_k^\dagger b_k, \quad (4)$$

$$H_I = \frac{1}{2}\sigma_z \sum_k g_k (b_k^\dagger + b_k), \quad (5)$$

where b_k^\dagger (b_k) is the creation (or annihilation) operator of the k th boson mode with frequency ω_k ; σ_x and σ_z are Pauli matrices to describe the spin system; ϵ is the bias, Δ is the bare tunneling and g_k is the coupling between the spin and the boson environment. Notice that g and g_k are two different quantities and there is no correlation between them. The boson environment of the SBM is described by the Lorentzian structured spectral density, and it reads [13, 14, 15, 16]

$$J(\omega) = \sum_k g_k^2 \delta(\omega - \omega_k) = \frac{2\alpha\omega\Omega^4}{(\Omega^2 - \omega^2)^2 + (2\pi\Gamma\omega\Omega)^2}, \quad (6)$$

in which $\alpha = \lim_{\omega \rightarrow 0} J(\omega)/(2\omega) = 8\Gamma g^2/\Omega^2$ is the dimensionless coupling constant.

Our model starts with the SBM in (2). In order to take into account the correlation between the spin and bosons, a unitary transformation is applied to H to obtain $H' = \exp(S)H \exp(-S)$, where the generator $S = \sum_k [(g_k/(2\omega_k))] (b_k^\dagger - b_k)[\xi_k \sigma_z + (1 - \xi_k)\sigma_0]$. Here we introduce a constant σ_0 and a k -dependent function ξ_k , which will be determined later. We rewrite the transformed $H' = H'_0 + H'_1 + H'_2$ as

$$\begin{aligned} H'_0 = & -\frac{1}{2}\eta\Delta\sigma_x + \frac{1}{2}\epsilon\sigma_z + \sum_k \omega_k b_k^\dagger b_k \\ & - \sum_k \frac{g_k^2}{4\omega_k} \xi_k (2 - \xi_k) - \sum_k \frac{g_k^2}{4\omega_k} \sigma_0^2 (1 - \xi_k)^2, \end{aligned} \quad (7)$$

$$H'_1 = \frac{1}{2} \sum_k g_k (1 - \xi_k) (b_k^\dagger + b_k) (\sigma_z - \sigma_0) - \frac{i\sigma_y}{2} \eta \Delta X, \quad (8)$$

$$\begin{aligned}
H'_2 = & -\frac{1}{2}\Delta\sigma_x(\cosh X - \eta) - \frac{1}{2}\Delta i\sigma_y(\sinh X - \eta X) \\
& - \sum_k \frac{g_k^2}{2\omega_k}\sigma_0(1 - \xi_k)^2(\sigma_z - \sigma_0),
\end{aligned} \tag{9}$$

where $X \equiv \sum_k (g_k \xi_k / \omega_k) (b_k^\dagger - b_k)$, and η is the thermodynamic average of $\cosh X$, as

$$\begin{aligned}
\eta = & Z^{-1} \text{Tr} [\exp(-\beta H) \cosh X] \\
= & \exp \left[- \sum_k \frac{g_k^2}{2\omega_k^2} \xi_k^2 \coth \left(\frac{\omega_k}{2T} \right) \right],
\end{aligned} \tag{10}$$

with $Z = \text{Tr}[\exp(-\beta H)]$ and T is the temperature.

Since the spin and bosons are decoupled in H'_0 , it is exactly solvable. By a unitary matrix $U = \begin{pmatrix} u & v \\ v & -u \end{pmatrix}$, with $u = \sqrt{(1 - \epsilon/W)/2}$, $v = \sqrt{(1 + \epsilon/W)/2}$ and $W = \sqrt{\epsilon^2 + \eta^2 \Delta^2}$, the diagonalized $\tilde{H}_0 = U^\dagger H'_0 U$ reads

$$\begin{aligned}
\tilde{H}_0 = & -\frac{1}{2}W\sigma_z + \sum_k \omega_k b_k^\dagger b_k \\
& - \sum_k \frac{g_k^2}{4\omega_k} \xi_k (2 - \xi_k) - \sum_k \frac{g_k^2}{4\omega_k} \sigma_0^2 (1 - \xi_k)^2.
\end{aligned} \tag{11}$$

The eigenstate of \tilde{H}_0 is the direct product $|\{n_k\}, \pm\rangle$, where $|\pm\rangle$ are the eigenstates of σ_z with eigenvalues ± 1 respectively, and $|\{n_k\}\rangle$ are the eigenstates of bosons with n_k phonons for the mode k . The ground state of \tilde{H}_0 is $|g_0\rangle = |\{0_k\}, +\rangle$ and the lowest excited states are $|\{0_k\}, -\rangle$, $|\{1_k\}, +\rangle$ and $|\{1_k\}, -\rangle$.

Similarly, we make the transformations to get $\tilde{H}_1 = U^\dagger H'_1 U$ and $\tilde{H}_2 = U^\dagger H'_2 U$, which are treated as perturbation and they should be as small as possible. For this purpose, it's determined as $\sigma_0 = -\epsilon/W$ and $\xi_k = \omega_k/(\omega_k + W)$. Thus

$$\begin{aligned}
\tilde{H}_1 = & \frac{1}{2}(1 - \sigma_z) \sum_k Q_k (b_k^\dagger + b_k) \\
& + \frac{1}{2} \sum_k V_k \left[b_k^\dagger (\sigma_x + i\sigma_y) + b_k (\sigma_x - i\sigma_y) \right],
\end{aligned} \tag{12}$$

where $Q_k = g_k [\epsilon/(\omega_k + W)]$ and $V_k = g_k [\eta\Delta/(\omega_k + W)]$. In the SBM, $g_k \ll \Delta$. Q_k and V_k can be viewed as the renormalized spin-bath coupling, and they are always smaller than g_k and even smaller for the high frequencies. Obviously, $\tilde{H}_1|g_0\rangle = 0$. Under the eigenbasis of \tilde{H}_0 , \tilde{H}_1 has only off-diagonal terms and in the lowest states, it is $\langle\{0_k\}, -|\tilde{H}_1|\{1_k\}, +\rangle = V_k$, $\langle\{0_k\}, -|\tilde{H}_1|\{1_k\}, -\rangle = Q_k$ and $\langle\{1_k\}, -|\tilde{H}_1|\{1_{k'}\}, +\rangle = 0$. Meanwhile, the terms in \tilde{H}_2 are related to the multi-boson transition and their contributions to the physical quantities are to the fourth order of g_k ($O(g_k^4)$). These are key points in our approach. The transformed Hamiltonian is approximated as

$$\begin{aligned}
\tilde{H} = & \tilde{H}_0 + \tilde{H}_1 + \tilde{H}_2 \\
\approx & \tilde{H}_0 + \tilde{H}_1
\end{aligned} \tag{13}$$

in the following. Meanwhile, the previous treatment is an extension to the one proposed by Ref. [28], while our generator S and the second unitary transformation are different. However, the k -dependent function ξ_k and decomposing the Hamiltonian into three parts are with the same spirit and they have been discussed detailedly in Ref. [28].

Thus, the ground energy of \tilde{H} is just the same as that of \tilde{H}_0 and it is determined as

$$E_g = -\frac{1}{2}W - \sum_k \frac{g_k^2}{4\omega_k} \left[1 - \left(\frac{\eta\Delta}{\omega_k + W} \right)^2 \right]. \quad (14)$$

The Hamiltonian H in (2) can be solved exactly in two limits: one is the weak coupling limit with $E_g(\alpha \rightarrow 0) = -\sqrt{\Delta^2 + \epsilon^2}/2$ and the other is the zero tunneling limit with $E_g(\Delta \rightarrow 0) = -|\epsilon|/2 - \sum_k g_k^2/(4\omega_k)$. The ground energies in (14) are the same in both limits.

Up to now, the deduction is independent of any specific spectral density and it is not restricted to zero temperature. In the following, the treatment is at zero temperature. As shown in H'_0 , η is the renormalized tunneling factor. In the limit of zero temperature, it is

$$\eta = \exp \left[- \int_0^\infty \frac{J(\omega)d\omega}{2(\omega + W)^2} \right]. \quad (15)$$

The integration in (15) can be done to the end, analytically. In the case of zero bias ($\epsilon = 0$), η has the same expression as Huang's and similarly positive change of the tunneling frequency can be predicted when $\Delta \sim \Omega$, which fails by adiabatic approach [26]. Generally, the renormalized tunneling factor η is larger than 0, which means that there is an effective tunneling between the two states of the qubit in realistic situation. If the renormalized tunneling factor suddenly changes to 0, the localized-delocalized transition happens and the qubit will be localized in one of the two states where it is located before the transition.

Fig. 1 shows numerical results of η as a function of α . For larger Γ (eg. 0.15, 0.3), one can see that η suddenly goes to zero at the localized-delocalized transition point $\alpha = \alpha_L$, where $\eta = 0$ for all $\alpha \geq \alpha_L$. While for smaller Γ (eg. 0.01), η gradually goes to zero, and we set the cutting at the value $\eta = 0.0001$, which is small enough.

A phase diagram of the delocalized-localized transition point α_L vs. bias ϵ is plotted in Fig. 2 with different Γ ($=0.01, 0.02, 0.05, 0.1$) and different detunings Δ/Ω ($=0.5, 1$). The area of $\alpha < \alpha_L$ is called the "localized phase", and the area of $\alpha > \alpha_L$ the "delocalized phase". It shows that α_L increases with increasing ϵ and it is almost the same for different Δ 's. The change of α_L is remarkable for larger Γ or smaller ϵ . Therefore, one way by applying a small bias to the qubit can be used to read out the already localized qubit state, since it will greatly increases α_L and the qubit will be shifted from the localized state to the delocalized one.

3. Density operator and master equation

In the Schrödinger picture, the density operator of the SBM is denoted as $\rho_{\text{SB}}(t)$ for the Hamiltonian H in (2) and the density operator for \tilde{H} in (13) is $\tilde{\rho}_{\text{SB}}(t) = U^\dagger \exp(S) \rho_{\text{SB}}(t) \exp(-S) U$, where the subscript ‘SB’ denotes the total spin-boson system. In the following, it will be analyzed in the interaction picture, denoting by a superscript ‘I’ in the operator. \tilde{H}_0 is treated as the unperturbed part and \tilde{H}_1 is really a good perturbed part. Moreover, in the interaction picture, it is assumed that the density operator for \tilde{H} is $\tilde{\rho}_{\text{SB}}^{\text{I}}(t) = \tilde{\rho}_{\text{S}}^{\text{I}}(t) \rho_{\text{B}}$, where $\tilde{\rho}_{\text{S}}^{\text{I}}(t) = \text{Tr}_{\text{B}} \tilde{\rho}_{\text{SB}}^{\text{I}}(t)$ is the reduced density operator. Within Born approximation (only keeping the second order of \tilde{H}_1), we can obtain the non-Markovian master equation for the reduced density operator

$$\frac{d}{dt} \tilde{\rho}_{\text{S}}^{\text{I}}(t) = - \int_0^t \text{Tr}_{\text{B}} [\tilde{H}_1(t), [\tilde{H}_1(t'), \tilde{\rho}_{\text{S}}^{\text{I}}(t') \rho_{\text{B}}]] dt', \quad (16)$$

where $\tilde{H}_1(t)$ is denoted as the perturbed part \tilde{H}_1 in the interaction picture. Since the renormalized spin-bath coupling Q_k and V_k in \tilde{H}_1 are always smaller than g_k , it makes our Born approximation nontrivial and more reasonable by comparing with the common used Born approximation [29, 30], which directly does the perturbation to the second order of H_1 in (2).

The master equation in (16), without Markovian approximation, can be done to the end with a Laplace transformation and an inverse-Laplace transformation. Changing from the interaction picture back to the Schrödinger picture, denoting the reduced density operator in the Schrödinger picture as $\tilde{\rho}_{\text{S}}(t) = \begin{pmatrix} \tilde{\rho}_{11}(t) & \tilde{\rho}_{12}(t) \\ \tilde{\rho}_{21}(t) & \tilde{\rho}_{22}(t) \end{pmatrix}$ for \tilde{H} , at zero temperature, we obtain

$$\tilde{\rho}_{21}(t) = \frac{\tilde{\rho}_{21}(0)}{2\pi} \int_{-\infty}^{\infty} \frac{i \exp(-i\omega t) d\omega}{\omega - W - \Sigma(\omega) + i\Gamma(\omega)}, \quad (17)$$

and

$$\tilde{\rho}_{22}(t) = \frac{\tilde{\rho}_{22}(0)}{2\pi} \int_{-\infty}^{\infty} \frac{i \exp(-i\omega t) d\omega}{\omega - \Sigma'(\omega) + i\Gamma'(\omega)}. \quad (18)$$

Abbreviations are used in (17) and (18), as

$$\Gamma(\omega) = \gamma(\omega) + \frac{\epsilon^2}{\eta^2 \Delta^2} \gamma(\omega - W), \quad (19)$$

$$\Sigma(\omega) = R(\omega) + \frac{\epsilon^2}{\eta^2 \Delta^2} R(\omega - W), \quad (20)$$

and

$$\Gamma'(\omega) = \gamma(W + \omega) + \gamma(W - \omega), \quad (21)$$

$$\Sigma'(\omega) = R(W + \omega) - R(W - \omega), \quad (22)$$

where $R(\omega)$ and $\gamma(\omega)$ are real and imaginary parts of $\sum_k V_k^2 / (\omega - i0^+ - \omega_k)$ (0^+ is a positive infinitesimal introduced by the inverse-Laplace transformation),

$$R(\omega) = \sum_{\mathbf{k}} \frac{V_k^2}{(\omega - \omega_{\mathbf{k}})} = \int_0^\infty \frac{\eta^2 \Delta^2 J(\omega') d\omega'}{(\omega - \omega')(\omega' + W)^2}, \quad (23)$$

$$\gamma(\omega) = \pi \sum_{\mathbf{k}} V_k^2 \delta(\omega - \omega_{\mathbf{k}}) = \frac{\pi \eta^2 \Delta^2 J(\omega)}{(\omega + W)^2}, \quad (24)$$

respectively. Besides, two other terms in $\tilde{\rho}_S(t)$ are $\tilde{\rho}_{12}(t) = [\tilde{\rho}_{21}(t)]^\dagger$ and $\tilde{\rho}_{11}(t) = 1 - \tilde{\rho}_{22}(t)$. Since the specific form of $J(\omega)$ is not involved, therefore, an analytical expression of the reduced density operator $\tilde{\rho}_S(t)$ is offered and it is independent of any specific spectral density.

We assume the initial density operator at $t = 0$ is $\rho_{SB}(0) = \exp(-S) |+\rangle \langle +| \rho_B \exp(S)$. Thus, the corresponding initial reduced density operator for \tilde{H} in (13) is

$$\tilde{\rho}_S(0) = \frac{1}{2} \begin{pmatrix} 1 - \epsilon/W & \eta\Delta/W \\ \eta\Delta/W & 1 + \epsilon/W \end{pmatrix}. \quad (25)$$

4. Non-equilibrium dynamics and the physical interpretation

For the SBM, it is common to evaluate the non-equilibrium dynamics $P(t)$, as this is the quantity of interest in the experiments. $P(t)$ is also called the population difference. Following the unitary transforms, it is determined as

$$\begin{aligned} P(t) &= \text{Tr}_S (\text{Tr}_B (\rho_{SB}(t) \sigma_z)) \\ &= \text{Tr}_S (\text{Tr}_B (\exp(-S) U \tilde{\rho}_{SB}(t) U^\dagger \exp(S) \sigma_z)) \\ &= \frac{\epsilon}{W} [2\tilde{\rho}_{22}(t) - 1] + \frac{2\eta\Delta}{W} \text{Re} [\tilde{\rho}_{21}(t)]. \end{aligned} \quad (26)$$

Substituting (17) and (18) into (26) with the initial condition in (25), the dynamics reads

$$\begin{aligned} P(t) &= \frac{2\epsilon}{\pi W} \left(1 + \frac{\epsilon}{W}\right) \int_0^\infty d\omega \frac{\cos(\omega t) \Gamma'(\omega)}{[\omega - \Sigma'(\omega)]^2 + [\Gamma'(\omega)]^2} \\ &+ \frac{\eta^2 \Delta^2}{\pi W^2} \int_0^\infty d\omega \frac{\cos(\omega t) \Gamma(\omega)}{[\omega - W - \Sigma(\omega)]^2 + [\Gamma(\omega)]^2} - \frac{\epsilon}{W}. \end{aligned} \quad (27)$$

Thus, we end up at an exact analytical expression of the non-Markovian dynamics $P(t)$ in (27). As time goes to infinity, we have the dynamics at the long time limit $P(t \rightarrow \infty) = -\epsilon/W$.

4.1. Spectrum of the non-Markovian dynamics

In order to get insight into the dominant frequencies of $P(t)$, a Fourier transform is applied to (27) according to

$$S(\omega) \equiv \int_{-\infty}^{\infty} dt \cos(\omega t) P(t). \quad (28)$$

The spectrum $S(\omega)$ is an even function and for $\omega \geq 0$, it is written as

$$S(\omega) = \frac{2\epsilon}{W} \left(1 + \frac{\epsilon}{W}\right) \frac{\Gamma'(\omega)}{[\omega - \Sigma'(\omega)]^2 + [\Gamma'(\omega)]^2} + \frac{\eta^2 \Delta^2}{W^2} \frac{\Gamma(\omega)}{[\omega - W - \Sigma(\omega)]^2 + [\Gamma(\omega)]^2} - \frac{2\pi\epsilon}{W} \delta(\omega). \quad (29)$$

The frequency property of the dynamics $P(t)$ can be analyzed by $S(\omega)$ directly. On one hand, the first two terms in (29) are Lorentzian-like functions. On the other hand, $\gamma(\omega)$ is small when g is small or ω is away from Ω , thus $\Gamma(\omega)$ and $\Gamma'(\omega)$, which are functions related to $\gamma(\omega)$, are usually small. Therefore, the dominant frequencies of $S(\omega)$ should be the solutions ω_p of the equation

$$\omega - W - \Sigma(\omega) = 0, \quad (30)$$

and the solutions $\omega_{p'}$ of the equation

$$\omega - \Sigma'(\omega) = 0. \quad (31)$$

Since the dissipative environment generally adds shift and width to the dominant frequencies, we can investigate the physical nature in the limit of small HO-environment coupling ($\Gamma \rightarrow 0$). Consequently, the spectral density $J(\omega)$ in (6) goes to $(4g^2\Omega/\omega) [\delta(\omega - \Omega) + \delta(\omega + \Omega)]$ and $R(\omega)$ in (23) goes to $4g^2\eta^2\Delta^2/[(\omega - \Omega)(\Omega + W)^2]$. Therefore, according to (30) and (20), the dominant frequencies ω_p are solutions to the equation

$$\omega - W = \frac{4g^2}{(\Omega + W)^2} \left[\frac{\eta^2 \Delta^2}{\omega - \Omega} + \frac{\epsilon^2}{\omega - \Omega - W} \right]. \quad (32)$$

The equation (32) can be solved exactly. If $g^2\epsilon^2/[\Delta^2(\Omega + W)^2] \ll 1$, ω_p can be simplified and approximated as

$$\omega_{p1,2} \cong \frac{\Omega + W}{2} \pm \sqrt{\left(\frac{\Omega - W}{2}\right)^2 + \frac{4g^2\eta^2\Delta^2}{(\Omega + W)^2}} \quad (33)$$

where the subscripts '1, 2' relating to the sign '+, -', respectively, and

$$\omega_{p3} \cong (\Omega + W) + \frac{W4g^2\epsilon^2}{\Omega W(\Omega + W)^2 - 4g^2\eta^2\Delta^2}. \quad (34)$$

Similarly, according to (31) and (22), the dominant frequencies $\omega_{p'}$ are exactly solvable, as

$$\omega_{p'1} = 0 \quad (35)$$

and

$$\omega_{p'2,3} = \pm \sqrt{(W - \Omega)^2 + \frac{8g^2\eta^2\Delta^2}{(\Omega + W)^2}}. \quad (36)$$

Since $S(\omega)$ is an even function, we only need to consider the non-negative part ($\omega \geq 0$). Thus, the negative one ($\omega_{p'3}$) of the solutions $\omega_{p'}$ in (36) is discarded. Consequently, for non-zero bias, there are five dominant frequencies: $\omega_{p'1} = 0$, $\omega_{p'2}$, ω_{p1} , ω_{p2} , ω_{p3} .

For zero bias ($\epsilon = 0$), we have $\Gamma(\omega) = \gamma(\omega)$, $\Sigma(\omega) = R(\omega)$ and

$$S(\omega) = \frac{\eta^2\Delta^2}{W^2} \frac{\Gamma(\omega)}{[\omega - W - R(\omega)]^2 + [\gamma(\omega)]^2} \quad (37)$$

for the non-negative part $\omega \geq 0$. Similarly, the dominant frequencies can be determined but with only two frequencies ω_{p1} and ω_{p2} , which are the exactly solvable solutions of $\omega - W - R(\omega) = 0$, as

$$\omega_{p1,2} = \frac{\Omega + W}{2} \pm \sqrt{\left(\frac{\Omega - W}{2}\right)^2 + \frac{4g^2\eta^2\Delta^2}{(\Omega + W)^2}}. \quad (38)$$

It is consistent with Huang's results (see equation (17) in Ref. [26]). Compared to unbiased case, the effect of finite bias is three additional dominant frequencies: $\omega_{p'1} = 0$, $\omega_{p'2}$, ω_{p3} .

Since the renormalized tunneling in the limit of small HO-environment coupling is

$$\eta = \exp\left[-\frac{2g^2}{(\Omega + W)^2}\right] \cong 1, \quad (39)$$

the resonance condition is $\Omega = W_0 = \sqrt{\Delta^2 + \epsilon^2} \cong W$. For near resonance $\Omega = W$, (33) can be simplified and approximated as

$$\omega_{p1,2} \cong \Omega \pm \frac{\eta\Delta}{\Omega}g. \quad (40)$$

For zero bias, there are only two dominant frequencies $\omega_{p1,2} = \Omega \pm g$ according to (38), which is consistent to the result of the simple exactly solvable Jaynes-Cummings model [31]. Moreover, for $\Omega = W$ with finite bias, (36) can be simplified as

$$\omega_{p'2} = \frac{\sqrt{2}\eta\Delta}{\Omega}g. \quad (41)$$

In the case of finite detunings $|\Omega - W| > 0$, with small qubit-HO coupling $g \ll \Delta, \Omega$, (33) and (36) can be simplified and approximated as

$$\omega_{p1,2} \cong W + \frac{4g^2\eta^2\Delta^2}{(W - \Omega)(\Omega + W)^2} \quad (42)$$

or

$$\Omega + \frac{4g^2\eta^2\Delta^2}{(\Omega - W)(\Omega + W)^2}, \quad (43)$$

(in (42) and (43), the larger one is ω_{p1} and vice versa) and

$$\omega_{p'2} \cong |W - \Omega| + \frac{4g^2\eta^2\Delta^2}{|W - \Omega|(\Omega + W)^2}. \quad (44)$$

It is clear to show the physics of all these dominant frequencies: $\omega_{p'1} = 0$ (35) is a relaxation peak, ω_{p1} and ω_{p2} are related to the renormalized energy difference of the qubit in (42) and the energy of the HO in (43), and $\omega_{p'2}$ is related to the energy difference of the qubit and the HO in (44). Meanwhile, ω_{p3} is related to the summation of the qubit energy W and the HO energy Ω as shown in (34). Therefore, for small qubit-HO coupling, although ω_{p3} and $\omega_{p'2}$ are not exactly the summation or the difference between W and Ω , we might still call $\omega_{p'2}$ “beat frequency” and ω_{p3} “sum frequency”.

4.2. Spectrum of the qubit-HO system

Before exploring the exact spectrum $S(\omega)$ corresponding to the non-Markovian $P(t)$ in realistic situation, as an alternative view to (2), we will briefly investigate the energy spectrum of the equivalent qubit-HO-environment model (1), which is a physically clearer way. Since the environment generally adds shift and width to the dominant frequencies, to get a rough idea, the qubit-HO-environment model without HO-environment coupling ($\Gamma = 0$) is investigated here, and the qubit-HO Hamiltonian reads

$$H_{\text{q-HO}} = -\frac{\Delta}{2}\sigma_x + \frac{\epsilon}{2}\sigma_z + \Omega A^\dagger A + (A^\dagger + A)g\sigma_z. \quad (45)$$

If the qubit-HO is decoupled ($g = 0$), (45) is exactly solvable. By applying a unitary matrix to $H_{\text{q-HO}}$, it can be diagonalized as

$$H_{\text{q-HO}} = -\frac{W_0}{2}\sigma_z + \Omega A^\dagger A. \quad (46)$$

where $W_0 = \sqrt{\epsilon^2 + \Delta^2}$. Thus, the spectrum of the decoupled qubit-HO without environment is exactly shown, with eigenbasis $|n, \pm\rangle$, where $|n\rangle$ denotes the eigenstates of HO with n ($n = 0, 1, \dots, \infty$) phonons and $|\pm\rangle$ denotes the eigenstates of σ_z with eigenvalues ± 1 respectively.

If the qubit-HO is switched on ($g \neq 0$), (45) can be solved with exact numerical diagonalization, with eigenbasis denoting as $|j\rangle$ ($j = 0, 1, \dots, \infty$).

To further explore the instinct of the coupled qubit-HO system, an analytical deduce beyond RWA is provided as follows. Since (45) has similar form to (2) when removing the summation and the multimode index k and substituting $\omega_k \rightarrow \Omega$, $b_k^\dagger \rightarrow A^\dagger$, $b_k \rightarrow A$ and $g_k/2 \rightarrow g$, therefore, we make two similar unitary transformations $U'^\dagger \exp(S')H \exp(-S')U'$ to H in (45) with generator $S' = (g/\Omega)(A^\dagger - A)[\Omega\sigma_z/(\Omega + W') - \epsilon/(\Omega + W')]$ and $U' = \begin{pmatrix} u' & v' \\ v' & -u' \end{pmatrix}$, with $u' = \sqrt{(1 - \epsilon/W')/2}$, $v' = \sqrt{(1 + \epsilon/W')/2}$ and $W' = \sqrt{\epsilon^2 + \eta'^2 \Delta^2}$, and to the second order of the qubit-HO coupling g ($O(g^2)$), it reaches

$$\begin{aligned} H_{\text{q-HO}} \cong & -\frac{1}{2}W'\sigma_z + \Omega A^\dagger A \\ & + \frac{\epsilon g}{\Omega + W'}(1 - \sigma_z)(A^\dagger + A) \end{aligned}$$

$$\begin{aligned}
& + \frac{\eta' \Delta g}{\Omega + W'} [A^\dagger(\sigma_x + i\sigma_y) + A(\sigma_x - i\sigma_y)] \\
& - \frac{g^2(\Omega + 2W')}{(\Omega + W')^2} - \frac{g^2 \epsilon^2}{\Omega(\Omega + W')^2},
\end{aligned} \tag{47}$$

where $\eta' = \exp[-2g^2/(\Omega + W')^2]$. Note that $(1 - \sigma_z)|+\rangle = 0$. If the value $|\epsilon g/[\Delta(\Omega + W')]| \ll 1$, then the term $\epsilon g(1 - \sigma_z)(A^\dagger + A)/(\Omega + W')$ in (47) can be discarded. Therefore, $H_{\text{q-HO}}$ is exactly solvable analytically.

For zero bias ($\epsilon = 0$), Ref. [20] has used the Van Vleck perturbation up to the second order g and solved a Born-Markov master equation in the system's eigenbasis to get the dynamics $P(t) = \sum_n p_{nn}(t) + \sum_{n,m(n>m)} p_{nm}(t)$ with the phonon number $n, m = 0, 1, \dots, \infty$, and it proposes selection rules for zero bias: $p_{nn}(t)$ vanishes for any n , and the non-zero $p_{nm}(t)$ only exists for three cases: $|n_{\text{even}} - m_{\text{even}}| = 2$, $|n_{\text{odd}} - m_{\text{odd}}| = 2$, $n_{\text{even}} - m_{\text{odd}} = 3$ or $n_{\text{odd}} - m_{\text{even}} = 1$. When substituting $\epsilon = 0$ into (47), the Hamiltonian (47) is exactly solvable analytically. Following Ref. [20], the selection rules can be deduced similarly. The selection rules show that the transition between the lowest energy levels $|j\rangle$: $|0\rangle \leftrightarrow |1\rangle$ and $|0\rangle \leftrightarrow |2\rangle$ are allowed, $|1\rangle \leftrightarrow |2\rangle$ and $|0\rangle \leftrightarrow |3\rangle$ are forbidden. This offers a second way to explain why there are only two dominant frequencies for zero bias.

4.3. Results and discussion

The Markovian approximation of $P(t)$ is equivalent to approximate the integration in (17) and (18) by the residue theorem with single pole at $-2i\gamma_0$ and $\omega_0 - i\gamma_0$, respectively. It leads to

$$\begin{aligned}
P(t) &= \frac{\eta^2 \Delta^2}{W^2} \cos(\omega_0 t) \exp(-\gamma_0 t) \\
&+ \frac{\epsilon}{W} \left[\left(\frac{\epsilon}{W} + 1 \right) \exp(-2\gamma_0 t) - 1 \right],
\end{aligned} \tag{48}$$

where $\gamma_0 = \gamma(W)$ is the Weisskopf-Wigner approximation for the decay rate and $\omega_0 = W + \Sigma(W)$ ($\Sigma(W)$ is the level shift). In the long time limit, the Markovian dynamics is the same as the non-Markovian one.

In Fig. 3, in the case of zero bias ($\epsilon = 0$) with weak coupling ($\Delta = \Omega$, $g = 0.18\Omega$, $\alpha = 0.004$, $\Gamma = 0.0154$), our non-Markovian dynamics $P(t)$ and the corresponding spectrum $S(\omega)$ at zero temperature is compared with the ones by QUAPI [19], by VVBM [20] (the numerical results) and by NIBA [24] at low temperature $T = 0.1\Delta$. They show good agreement with both $P(t)$ and $S(\omega)$. The reasons of comparing to other results at the low temperature are: first, corresponding results at zero temperature by other methods are not found in literature; second, temperature gives a factor $\coth(\frac{\omega}{2T})$ for each frequency, and in a rough view $\coth(\frac{\omega}{2T}) \sim 1$ for typical frequencies (eg. $\omega = \Delta$) at $T = 0.1\Delta$; third, the temperature $T = 0.1\Delta$ is really low and the comparisons show that their properties are analogous.

From Fig. 4 to Fig. 6, at finite bias ($\epsilon = -0.5\Delta$, $g = 0.18\Delta$, $\Gamma = 0.0154$), our non-Markovian dynamics $P(t)$ and the corresponding spectrum $S(\omega)$ at zero temperature is

compared with the numerical results by VVBM [20] at low temperature $T = 0.1\Delta$ for three different situations: the qubit being at positive detunings with the HO ($\Omega = 1.5\Delta > W_0$), on resonance ($\Omega = W_0$), and negative detunings ($\Omega = 0.9\Delta < W_0$). Roughly, both the dynamics and the spectrum shows good agreement. Moreover, *our spectrum presents five dominant frequencies*: one relaxation dip (at $\omega = 0$), one dephasing dip (ω_{21}) and three dephasing peaks ($\omega_{10}, \omega_{20}, \omega_{30}$), where the four damping oscillation frequencies are related to the energy differences of the four lowest energy levels of the coupled qubit-HO system as shown in the insets and they have been verified by the exact numerical diagonalization of H_{q-HO} (45). Note that the symbols ω_{ij} denote the dominant frequencies of $S(\omega)$ relating to the energy difference of the energy levels $|i\rangle$ and $|j\rangle$ of the coupled qubit-HO system. Meanwhile, the dominant frequencies can also be well interpreted with the relaxation dip at $\omega = 0 \Leftrightarrow \omega_{p'1} = 0$ in (35), the dephasing peaks at $\omega_{10} \Leftrightarrow \omega_{p2}$ and $\omega_{20} \Leftrightarrow \omega_{p1}$ in (33), $\omega_{30} \Leftrightarrow \omega_{p3}$ in (34), and the dephasing dip at $\omega_{21} \Leftrightarrow \omega_{p'2}$ in (36). Since in Figs. 4 - 6 the qubit-HO coupling is small ($g = 0.18\Delta \ll \Delta, \Omega$), the expressions for ω_{p1} , ω_{p2} and $\omega_{p'2}$ can be written in simpler approximate forms, as: for on resonance in Fig. 5, $\omega_{10} \Leftrightarrow \omega_{p2}$ and $\omega_{20} \Leftrightarrow \omega_{p1}$ in (40), $\omega_{21} \Leftrightarrow \omega_{p'2}$ in (41); for off-resonance in Fig. 4 and Fig. 6, $\omega_{10} \Leftrightarrow \omega_{p2}$ and $\omega_{20} \Leftrightarrow \omega_{p1}$ relating to the renormalized energy difference of the qubit in (42) and relating to the energy of the HO in (43), $\omega_{21} \Leftrightarrow \omega_{p'2}$ relating to the energy difference of the qubit and the HO in (44).

In Ref. [20] by VVBM, it presents four dominant frequencies: one relaxation dip (at $\omega = 0$), one dephasing dip (ω'_{21}) and two dephasing peaks ($\omega'_{10}, \omega'_{20}$), and similar result is also claimed by QUAPI in Ref. [19] (see its Fig. 7). In order to distinguish the dominant frequencies by different methods and/or under different conditions, analogous symbols ω'_{ij} denote the dominant frequencies of numerical results by VVBM in Ref. [20] are employed. As comparison, neither [19] nor [20] presents the analogous dephasing peak(or dip) at ω_{30} , and to our knowledge, it is not shown in literature. In all the three figures, the width and height of the dephasing peak at ω_{20} matches quite well with the one at ω'_{20} , but our dephasing peak at ω_{10} and dephasing dip at ω_{21} are much higher and sharper, especially for on resonance in Fig. 5. Meanwhile, the dominant frequencies ω'_{ij} are nearly equal to the dominant frequencies ω_{ij} , but in detail ω'_{ij} are a bit larger than ω_{ij} . For on resonance in Fig. 5, our dephasing dip at ω_{21} has comparable weight with our dephasing peaks at ω_{10} and ω_{20} , which is qualitatively different from the ones by VVBM. Besides, we must admit that the dephasing peaks at ω_{30} shown in Fig. 4 to Fig. 6 are really small, which makes it difficult to discover. As a brief summary, there is a complete new dephasing peak presented in our spectrum and our dynamics and spectrum shows a good agreement with Ref. [20] roughly.

In order to compare our approach with VVBM in Ref. [20], g are all rather small in Figs. 4 - 6, as well as the corresponding α (all $\alpha < 0.005$). Nevertheless, our approach has no direct restriction in g and it can work with stronger α . Therefore, in Figs. 7 - 8, it presents with larger qubit-HO coupling ($g=0.7906\Omega$) and larger spin-bath coupling ($\alpha = 0.01, 0.05, 0.1$) for positive detunings ($\Omega = 2\Delta > W_0$) and near

resonance ($\Omega = \Delta \sim W_0$). The results for negative detunings are similar to the positive ones and the figure for negative detunings is not repeated. Likewise, the biased spectrum presents one relaxation peak (at $\omega = 0$) and four dephasing peaks ($\omega_{10}, \omega_{20}, \omega_{21}, \omega_{30}$). The dominant frequencies can be well interpreted with the energy differences of the four lowest energy levels of the coupled qubit-HO system as above. Similarly, they can also be well interpreted with the relaxation peak at $\omega = 0 \Leftrightarrow \omega_{p'1} = 0$ in (35), the dephasing peaks at $\omega_{10} \Leftrightarrow \omega_{p2}$ and $\omega_{20} \Leftrightarrow \omega_{p1}$ in (33), $\omega_{30} \Leftrightarrow \omega_{p3}$ in (34), and the dephasing dip at $\omega_{21} \Leftrightarrow \omega_{p'2}$ in (36). In contrast to the small qubit-HO coupling, the weight of the dephasing peaks at ω_{30} shown in Figs. 7 - 8 grows rather larger. For near resonance in Fig. 8, our dephasing peak at ω_{21} has comparable weight with our dephasing peaks at ω_{10} and ω_{20} and the weight of the dephasing peak at ω_{30} grows much larger than that for off-resonance in Fig. 7.

Meanwhile, the corresponding Markovian dynamics given by (48) are presented in Fig. 7 to show the long time limit. Moreover, in Fig. 8 with the same $\Delta = \Omega$, $g = 0.7906\Omega$ and $\epsilon = 0.1\Omega$, the effect with different Γ ($= 0.002, 0.01, 0.02$) is shown, as well as different corresponding α ($= 0.01, 0.05, 0.1$). The results show that the distributions of the dominant frequencies vary little, but with smaller Γ or α , the dephasing peaks will be higher and sharper and the dephasing will be smaller, which is physically reasonable.

The non-Markovian dynamics and the spectrum for zero bias ($\epsilon = 0$) in Figs. 3 - 8 show that the spectrum only presents two dephasing peaks ($\omega''_{10}, \omega''_{20}$) for zero bias, which is consistent with literature results and has been interpreted in two ways as shown above (with (38) or the selection rules). Similarly, ω''_{ij} are employed to denote the dominant frequencies for zero bias and they are related to the energy levels of the unbiased coupled qubit-HO system. Compared to zero bias, the effect of non-zero bias is shown in Figs. 4 - 8, i.e., three more resonances in the spectrum appear: the relaxation peak at $\omega = 0$, a third dephasing peak(dip) at ω_{21} and a fourth dephasing peak at ω_{30} . Besides, the dominant frequency ω''_{10} for zero bias is usually smaller than the biased one ω_{10} and the dephasing peak at ω''_{10} is usually higher.

For non-zero bias, at $\omega = 0$ and ω_{21} , it is clearly shown two dips for negative bias and two peaks instead for positive bias in Figs. 4 - 8. It can be interpreted as follows: $\omega = 0$ is mapped to $\omega_{p'1} = 0$ and ω_{21} is mapped to $\omega_{p'2}$; $\omega_{p'1}$ and $\omega_{p'2}$ are the solutions $\omega_{p'}$ of the equation (31); the equation (31) is from the first term of $S(\omega)$ in (29); the sign of the first term of $S(\omega)$ in (29) is the same with the bias ϵ . Similarly analysis can be done for the remainder three dominant frequencies. Therefore, there are always peaks at ω_{10}, ω_{20} and ω_{30} ; while at $\omega = 0$ and ω_{21} , there are peaks for positive bias ($\epsilon > 0$), dips for negative bias ($\epsilon < 0$).

As a brief summary to the biased spectrum $S(\omega)$ of the non-Markovian dynamics $P(t)$: there are five resonances, i.e., the relaxation peak(dip) at $\omega = 0$, one dephasing peak(dip) at $\omega = \omega_{21}$, three dephasing peaks at $\omega = \omega_{10}, \omega_{20}, \omega_{30}$, which are related to the energy differences of the four lowest energy levels of the coupled qubit-HO system. For the qubit being with the HO at positive detunings ($\Omega > W_0$), the dephasing peak

at $\omega = \omega_{10}$ and the relaxation peak(dip) at $\omega = 0$ are generally dominant; for on/near resonance ($\Omega \cong W_0$), the dephasing peaks(dip) at $\omega = \omega_{10}, \omega_{20}, \omega_{21}$ are generally dominant; for negative detunings ($\Omega < W_0$), if g is small, the dephasing peak at $\omega = \omega_{20}$ is generally dominant, otherwise, the peak at $\omega = \omega_{10}$ is dominant. A rough idea is that: the dominant frequency(ies) closer to the renormalized energy difference of the qubit (W_0) usually contribute(s) more weight.

Fig. 9 shows the dynamics with different α for non-zero bias. As usual, decay accompanies larger α . Our method works well for sufficient strong spin-bath coupling as long as $\alpha < \alpha_c$ (see Sec. 5) beyond weak coupling regime.

The sum rule of the non-Markovian dynamics is checked as shown in Table 1, and it is exactly satisfied with representative parameters for $\alpha < \alpha_c$.

5. Susceptibility and coherent-incoherent transition

The susceptibility $\chi(\omega) = -G(\omega)$, where $G(\omega)$ (obtained in the Appendix in detail) is the fourier transformation of the retarded Green's function $G(t) = -i\theta(t)Z^{-1}\text{Tr}\{\exp(-\beta H)[\sigma_z(t), \sigma_z]\}$, in which $\theta(t)$ is the unit step function. The imaginary part of $\chi(\omega)$ is $\chi''(\omega)$, as

$$\chi''(\omega) = \frac{\eta^2 \Delta^2}{W^2} \left\{ \frac{\Gamma(\omega)\theta(\omega)}{[\omega - W - \Sigma(\omega)]^2 + \Gamma^2(\omega)} - \frac{\Gamma(-\omega)\theta(-\omega)}{[\omega + W + \Sigma(-\omega)]^2 + \Gamma^2(-\omega)} \right\}, \quad (49)$$

and its real part $\chi'(\omega = 0)$ can be obtained by Kramers-Kronig relation, as

$$\chi'(\omega = 0) = \frac{2}{\pi} \int_0^\infty \frac{\chi''(\omega)}{\omega} d\omega. \quad (50)$$

Our approach can be checked by the Shiba's relation [32, 33, 34, 35]

$$\lim_{\omega \rightarrow 0} \frac{\chi''(\omega)}{J(\omega)} = \frac{\pi}{4} [\chi'(\omega = 0)]^2. \quad (51)$$

As long as $\alpha < \alpha_c$, the Shiba relation is exactly satisfied as shown in Table. 1 with representative parameters.

The susceptibility $\chi''(\omega)$ is the same as the second term of $S(\omega)$ in (29) for $\omega \geq 0$ and it is an odd function of ω . Usually $\chi''(\omega = 0) = 0$. While increasing α to a particular value α_c , a critical phase happens and $\chi''(\omega = 0) = \infty$. Meanwhile, $\Gamma(\omega) \propto \omega$ and we have checked that $[\omega - W - \Sigma(\omega)] \propto \omega$ when $\omega \rightarrow 0$. Thus, the coherent-incoherent transition point [1, 2] α_c is defined as the solution of

$$-W - \Sigma(0) = 0. \quad (52)$$

In Fig. 9, non-Markovian dynamics $P(t)$ and the susceptibility $\chi''(\omega)$ are shown with different α ($= 0.005, 0.05, 0.1, 0.2168$). Meanwhile, the coherent-incoherent transition point α_c ($= 0.21683229$) is calculated by (52). $P(t)$ exhibits much abundant oscillation for a weak α ($= 0.005$), beating oscillation for a moderate α ($= 0.05$), a

badly damping oscillation for a moderately strong α ($= 0.1$), and nearly pure damping for a sufficient strong α ($= 0.2168$) nearly equals to α_c . In the inset of Fig. 9, $\chi''(\omega)$ is plotted against ω , and the curve shows with three non-zero frequency peaks for all $\alpha < \alpha_c$. Increasing α from weak (0.005) to strong (0.2168), the peak at the smallest frequency moves rapidly close to $\omega = 0$ and the corresponding peak grows to a great value, and other peaks goes close to zero. When $\alpha < \alpha_c$, $\chi''(\omega = 0) = 0$. At $\alpha = \alpha_c$, $\chi''(\omega = 0) = \infty$. Therefore, the particular value α_c is the coherent-incoherent transition point.

In Fig. 10, phase diagrams of the coherent-incoherent transition point α_c vs. bias ϵ with different Γ are shown. The area of $\alpha < \alpha_c$ is called as the “coherent phase”, and the “incoherent phase” for $\alpha > \alpha_c$. As shown in Fig. 10(a) for near-resonance $\Delta = \Omega$, the changing curve of α_c vs. ϵ is an Ohmic-alike. α_c gradually increases with increasing bias, and it remarkably increases with increasing Γ . As shown in Fig. 10(b) for off-resonance $\Delta = 0.5\Omega$, the changing curve is nontrivial for small $\Gamma = 0.075$: one sharp peak exists around $\epsilon = 0.0655\Omega$ and the curve at the ends behaves Ohmic-alike. The sharp peak is substituted by a smooth kink for $\Gamma = 0.0762$. While for $\Gamma = 0.08, 0.1$, the kink disappears and the whole curves behave Ohmic-alike. More results show that when decreasing Γ (eg. $\Gamma < 0.075$) the sharp peak grows much sharper and higher, and the corresponding bias of the peak becomes smaller. Under smaller Γ , a significant difference of α_c between the steep area at finite bias and the platform area with zero bias might be utilized, eg. reading out the qubit state.

6. Conclusions

We have investigated the biased SBM with a Lorentzian spectral density by a new analytical approach at zero temperature. An equivalent description of the system is provided by a biased qubit coupled through a HO to an Ohmic environment. The starting point is the general SBM Hamiltonian (2) without RWA. We have applied two unitary transformations to the Hamiltonian and the non-Markovian master equation within the nontrivial Born approximation to get an expression for the density operator. With the density operator, we have provided analytical expressions for the non-Markovian dynamics $P(t)$ and the corresponding spectrum $S(\omega)$. Meanwhile, the localized-delocalized transition point α_L and the coherent-incoherent transition point α_c are determined, which have not been provided so far (except α_c with zero bias by Ref. [26]), as well as the analytical ground energy, the renormalized tunneling factor η and the susceptibility $\chi''(\omega)$. The sum rule and the Shiba relation are carefully checked and they are exactly satisfied as long as $\alpha < \alpha_c$.

The biased dynamics and the corresponding spectrum are key topics in this paper. Both for biased and unbiased, they have been compared with the results of the other groups and have shown good agreements. For non-zero bias, our spectrum presents *five dominant frequencies*: the relaxation peak(dip) at $\omega = 0$, one dephasing peak(dip) at $\omega = \omega_{21}$, three dephasing peaks at $\omega = \omega_{10}, \omega_{20}, \omega_{30}$, and *there is a new effect*: an

additional dephasing peak at $\omega = \omega_{30}$ presented in our spectrum. Our approach has no direct restriction on the qubit-HO coupling g . Therefore, it is a good way to investigate the dynamics in the little-studied strong qubit-HO coupling regime, especially in the static biased case, which has not been studied yet to our knowledge, as shown in Figs. 7-9. Moreover, the origin and the meanings of the dominant frequencies are well studied in two ways: providing analytical expressions for each dominant frequency in the limit conditions and comparing with the spectrum of the qubit-HO system. We've also discussed why it is sometimes peak and sometimes dip, as well as the weight distribution of the peaks(dips) and why there are only two dominant frequencies for unbiased. Meanwhile, fixing other parameters, the effect with different α and corresponding Γ is also shown. The dynamics at the long time limit is given analytically as $-\epsilon/W$, which is consistent with the Markovian dynamics.

In summary, we have provided analytical results for interesting physical quantities without Markovian approximation and our approach works well at arbitrary detunings: on/off-resonance, with/without bias and for sufficient strong spin-bath coupling as long as $\alpha < \alpha_c$. Admittedly, this approach is not suitable for very strong spin-bath coupling, e.g. $\alpha > \alpha_c$. Nevertheless, the coherent regime is the most interesting one in the field of quantum computation and quantum information.

Acknowledgement

This work was supported by the China National Natural Science Foundation (Grants No.90503007 and No.10734020).

Appendix

Following the transformation made to H to reach \tilde{H} , the retarded Green's function is

$$\begin{aligned} G(t) &= -i\theta(t)Z^{-1}\text{Tr}\{\exp(-\beta H)[\exp(iHt)\sigma_z\exp(-iHt),\sigma_z]\} \\ &= -i\theta(t)Z^{-1}\text{Tr}\left\{\exp(-\beta\tilde{H})\left(\frac{\epsilon^2}{W^2}[\sigma_z(t),\sigma_z] + \frac{\eta^2\Delta^2}{W^2}[\sigma_x(t),\sigma_x] \right. \right. \\ &\quad \left. \left. - \frac{\eta\Delta\epsilon}{W^2}[\sigma_z(t),\sigma_x] - \frac{\eta\Delta\epsilon}{W^2}[\sigma_x(t),\sigma_z]\right)\right\}. \end{aligned} \quad (\text{A.1})$$

The Fourier transformation of $G(t)$ is denoted as

$$\begin{aligned} G(\omega) &= \frac{\epsilon^2}{W^2}\langle\langle\sigma_z;\sigma_z\rangle\rangle + \frac{\eta^2\Delta^2}{W^2}\langle\langle\sigma_x;\sigma_x\rangle\rangle \\ &\quad - \frac{\eta\Delta\epsilon}{W^2}\langle\langle\sigma_z;\sigma_x\rangle\rangle - \frac{\eta\Delta\epsilon}{W^2}\langle\langle\sigma_x;\sigma_z\rangle\rangle, \end{aligned} \quad (\text{A.2})$$

where

$$\langle\langle A; B \rangle\rangle = -i\theta(t)Z^{-1}\text{Tr}\left\{\exp(-\beta\tilde{H})[\exp(i\tilde{H}t)A\exp(-i\tilde{H}t), B]\right\}$$

denotes the retarded Green's function which satisfies the following equation of motion,

$$\begin{aligned} \omega\langle\langle A; B \rangle\rangle &= \langle[A, B]\rangle + \left\langle\left\langle[A, \tilde{H}]; B\right\rangle\right\rangle, \\ \langle[A, B]\rangle &= Z^{-1}\text{Tr}\left\{\exp(-\beta\tilde{H})[A, B]\right\}. \end{aligned}$$

Thus, we can get the following equation chain:

$$\begin{aligned} \omega \langle \langle \sigma_x; \sigma_x \rangle \rangle &= W \langle \langle i\sigma_y; \sigma_x \rangle \rangle \\ &+ \sum_k Q_k \langle \langle i\sigma_y(b_k^\dagger + b_k); \sigma_x \rangle \rangle - \sum_k V_k \langle \langle \sigma_z(b_k^\dagger - b_k); \sigma_x \rangle \rangle, \end{aligned} \quad (\text{A.3})$$

$$\begin{aligned} \omega \langle \langle i\sigma_y; \sigma_x \rangle \rangle &= 2 \langle \sigma_z \rangle_{\tilde{H}_0} + W \langle \langle \sigma_x; \sigma_x \rangle \rangle \\ &+ \sum_k Q_k \langle \langle \sigma_x(b_k^\dagger + b_k); \sigma_x \rangle \rangle + \sum_k V_k \langle \langle \sigma_z(b_k^\dagger + b_k); \sigma_x \rangle \rangle, \end{aligned} \quad (\text{A.4})$$

$$\begin{aligned} \omega \langle \langle \sigma_x(b_k^\dagger + b_k); \sigma_x \rangle \rangle &= -\omega_k \langle \langle \sigma_x(b_k^\dagger - b_k); \sigma_x \rangle \rangle \\ &+ W \langle \langle i\sigma_y(b_k^\dagger + b_k); \sigma_x \rangle \rangle + Q_k \langle \langle i\sigma_y; \sigma_x \rangle \rangle, \end{aligned} \quad (\text{A.5})$$

$$\begin{aligned} \omega \langle \langle \sigma_x(b_k^\dagger - b_k); \sigma_x \rangle \rangle &= -\omega_k \langle \langle \sigma_x(b_k^\dagger + b_k); \sigma_x \rangle \rangle \\ &+ W \langle \langle i\sigma_y(b_k^\dagger - b_k); \sigma_x \rangle \rangle - Q_k \langle \langle \sigma_x; \sigma_x \rangle \rangle, \end{aligned} \quad (\text{A.6})$$

$$\begin{aligned} \omega \langle \langle i\sigma_y(b_k^\dagger + b_k); \sigma_x \rangle \rangle &= -\omega_k \langle \langle i\sigma_y(b_k^\dagger - b_k); \sigma_x \rangle \rangle \\ &+ W \langle \langle \sigma_x(b_k^\dagger + b_k); \sigma_x \rangle \rangle + Q_k \langle \langle \sigma_x; \sigma_x \rangle \rangle, \end{aligned} \quad (\text{A.7})$$

$$\begin{aligned} \omega \langle \langle i\sigma_y(b_k^\dagger - b_k); \sigma_x \rangle \rangle &= -\omega_k \langle \langle i\sigma_y(b_k^\dagger + b_k); \sigma_x \rangle \rangle \\ &+ W \langle \langle \sigma_x(b_k^\dagger - b_k); \sigma_x \rangle \rangle - Q_k \langle \langle i\sigma_y; \sigma_x \rangle \rangle, \end{aligned} \quad (\text{A.8})$$

where $\langle \sigma_z \rangle_{\tilde{H}_0} = \langle g_0 | \sigma_z | g_0 \rangle = 1$. We have already made the cutoff approximation for the equation chains at the second order of g_k . Besides, $\langle \langle \sigma_z; \sigma_x \rangle \rangle = 0$, $\langle \langle \sigma_z; \sigma_z \rangle \rangle = 0$, and $\langle \langle \sigma_x; \sigma_z \rangle \rangle = 0$. So the solution for $G(\omega)$ is

$$\begin{aligned} G(\omega) &= \frac{\eta^2 \Delta^2}{W^2} \left(\frac{1}{\omega - W - \sum_k V_k^2 / (\omega - \omega_k) - \sum_k Q_k^2 / (\omega - W - \omega_k)} \right. \\ &\quad \left. - \frac{1}{\omega + W - \sum_k V_k^2 / (\omega + \omega_k) - \sum_k Q_k^2 / (\omega + W + \omega_k)} \right). \end{aligned} \quad (\text{A.9})$$

References

- [1] Leggett A J, Chakravarty S, Dorsey A T, Fisher M P A, Garg A and Zwerger W 1987 *Rev. Mod. Phys.* **59** 1
- [2] Weiss U 1999 *Quantum Dissipative Systems* (Singapore: World Scientific)
- [3] Grifoni M and Haggi P 1998 *Phys. Rep.* **304** 229
- [4] Vion D, Aassime A, Cottet A, Joyez P, Pothier H, Urbina C, Esteve D and Devoret M H 2002 *Science* **296** 886
- [5] Yu Y, Han S, Chu X, Chu S-I and Wang Z 2002 *Science* **296** 889
- [6] Chiorescu I, Nakamura Y, Harmans C J P M and Mooij J E 2003 *Science* **299** 1869
- [7] Chiorescu I, Bertet P, Semba K, Nakamura Y, Harmans C J P M and Mooij J E 2004 *Nature* **431** 159

- [8] Imamoglu A, Awschalom D D, Burkard G, DiVincenzo D P, Loss D, Sherwin M and Small A 1999 *Phys. Rev. Lett.* **83** 4204
- [9] Martinis J M, Nam S, Aumentado J and Urbina C 2002 *Phys. Rev. Lett.* **89** 117901
- [10] Wallraff A, Schuster D I, Blais A, Frunzio L, Huang R S, Majer J, Kumar S, Girvin S M and Schoelkopf R J 2004 *Nature* **431** 162
- [11] Thorwart M, Hartmann L, Goychuk I and Hänggi P 2000 *J. Mod. Optic.* **47** 2905
- [12] van der Wal C H, ter Haar A C J, Wilhelm F K, Schouten R N, Harmans C J P M, Orlando T P, Lloyd S and Mooij J E 2000 *Science* **290** 773
- [13] Garg A, Onuchic J N and Ambegaokar V 1985 *J. Chem. Phys.* **83** 4491
- [14] Tian L, Lloyd S and Orlando T P 2002 *Phys. Rev. B* **65** 144516
- [15] van der Wal C H, Wilhelm F K, Harmans C J P M and Mooij J E 2003 *Eur. Phys. J. B* **31** 111
- [16] Robertson T L, Plourde B L T, Hime T, Linzen S, Reichardt P A, Wilhelm F K and Clarke J 2005 *Phys. Rev. B* **72** 024513
- [17] Goorden M C, Thorwart M and Grifoni M 2004 *Phys. Rev. Lett.* **93** 267005
- [18] Goorden M C, Thorwart M and Grifoni M 2005 *Eur. Phys. J. B* **45** 405-17
- [19] Thorwart M, Paladino E and Grifoni M 2004 *Chem. Phys.* **296** 333
- [20] Hausinger J and Grifoni M 2008 *New. J. Phys.* **10** 115015
- [21] Kleff S, Kehrein S and von Delft J 2003 *Physica E* **18** 343-5
- [22] Wilhelm F K, Kleff S and von Delft J 2004 *Chem. Phys.* **296** 345
- [23] Kleff S, Kehrein S and von Delft J 2004 *Phys. Rev. B* **70** 014516
- [24] Nesi F, Grifoni M and Paladino E 2007 *New. J. Phys.* **9** 316
- [25] Brito F and Caldeira A O 2008 *New. J. Phys.* **10** 115014
- [26] Huang P H and Zheng H 2008 *J. Phys.-Condes. Matter* **20** 8
- [27] Stauber T and Mielke A 2003 *J. Phys. A: Math. Gen.* **36** 2707-36
- [28] Zheng H 2004 *EUR.PHYS.J.B.* **38** 559
- [29] Burkard G 2009 *Phys. Rev. B* **79** 125317
- [30] DiVincenzo D P and Loss D 2005 *Phys. Rev. B* **71** 035318
- [31] Jaynes E T and Cummings F W 1963 *P. IEEE* **51** 89
- [32] Sassetti M and Weiss U 1990 *Phys. Rev. A* **41** 5383
- [33] Sassetti M and Weiss U 1990 *Phys. Rev. Lett.* **65** 2262
- [34] Costi T A and Kieffer C 1996 *Phys. Rev. Lett.* **76** 1683
- [35] Costi T A 1998 *Phys. Rev. Lett.* **80** 1038

Figure Captions

Fig. 1 (color on the web) The renormalized tunneling factor η vs. α . It shows that η goes to zero gradually with smaller Γ and it goes to zero suddenly with larger Γ . A slight bias such as $\epsilon = 0.0002\Omega$ can be used to change the curve effectively. The inset is a magnification part.

Fig. 2 (color on the web) Phase diagram of the localized-delocalized transition point α_L vs. ϵ . It shows that α_L is almost the same with different Δ and the curve changes rapidly for larger Γ and/or smaller ϵ . Parameters: near-resonance $\Delta = \Omega$, $\Gamma = 0.01, 0.02, 0.05, 0.1$; off-resonance $\Delta = 0.5\Omega$, $\Gamma = 0.01, 0.02, 0.05, 0.1$.

Fig. 3 (color on the web) For zero bias ($\epsilon = 0$), non-Markovian dynamics $P(t)$ and its corresponding spectrum $S(\omega)$ at zero temperature show good agreements with results by QUAPI [19], VVBM [20] and NIBA [24] at low temperature $T = 0.1\Delta$. Inset (1) is a magnification part and inset (2) is $S(\omega)$ vs. ω . Parameters: $\Delta = \Omega$, $g = 0.18\Omega$, $\alpha = 0.004$, $\Gamma = 0.0154$.

Fig. 4 (color on the web) For off-resonance $\Omega = 1.5\Delta$ with $\epsilon = -0.5\Delta$, (a) non-Markovian dynamics $P(t)$ and (b) its corresponding spectrum $S(\omega)$ at zero temperature shows good agreement with VVBM [20] at low temperature $T = 0.1\Delta$. In detail, our spectrum presents one relaxation dip (at $\omega = 0$), one dephasing dip (ω_{21}) and three dephasing peaks ($\omega_{10}, \omega_{20}, \omega_{30}$). The dominant frequency ω_{30} is new. Moreover, the height of our peak at ω_{10} and dip at ω_{21} is nearly twice the ones by VVBM. For zero bias, there are only two dephasing peaks. Insets: The inset in (a) and insets (1)~(3) in (b) present magnification parts. Inset (4) in (b) presents the schematic energy levels of the qubit-HO system with finite bias, where the dashed lines on the left part for the uncoupled ($g = 0$) and the solid lines on the right part are numerical exact results for the coupled. Our dominant frequencies are related to the energy differences of the coupled qubit-HO system with numerical calculation. Parameters: $g = 0.18\Delta$, $\Gamma = 0.0154$, $\alpha = 0.00177$.

Fig. 5 (color on the web) For on-resonance $\Omega = W_0 = \sqrt{\Delta^2 + \epsilon^2}$ with $\epsilon = -0.5\Delta$, (a) non-Markovian dynamics $P(t)$ and (b) its corresponding spectrum $S(\omega)$ at zero temperature shows good agreement with VVBM [20] at low temperature $T = 0.1\Delta$.

Similarly to Fig. 4, our spectrum presents five dominant frequencies ($\omega = 0, \omega_{10}, \omega_{20}, \omega_{21}, \omega_{30}$) and the dominant frequency ω_{30} is new. Our dephasing dip at ω_{21} is much deeper and sharper than the ones by VVBM. Our dip at ω_{21} has comparable weight with our dephasing peaks at ω_{10} and ω_{20} , which is qualitatively different from the ones by VVBM. For zero bias, there are only two dephasing peaks. Insets: The inset in (a) and inset (1) in (b) presents magnification parts. Inset (2) in (b) presents the schematic energy levels of the qubit-HO system with finite bias, where the left dashed lines are for the uncoupled and the right solid lines are for the coupled. Our dominant frequencies are related to the energy differences of the coupled qubit-HO system with numerical calculation. Parameters: $g = 0.18\Delta$, $\Gamma = 0.0154$, $\alpha=0.00319$.

Fig. 6 (color on the web) For off-resonance $\Omega = 0.9\Delta$ with $\epsilon = -0.5\Delta$, (a) non-Markovian dynamics $P(t)$ and (b) its corresponding spectrum $S(\omega)$ at zero temperature shows good agreement with VVBM [20] at low temperature $T = 0.1\Delta$. Similarly to Fig. 4, our spectrum presents five dominant frequencies ($\omega = 0, \omega_{10}, \omega_{20}, \omega_{21}, \omega_{30}$) and the dominant frequency ω_{30} is new. Moreover, our peaks (or dips) are a bit sharper and higher than the ones by VVBM. For zero bias, there are only two dephasing peaks. Insets: The inset in (a) and inset (1) in (b) presents magnification parts. Inset (2) in (b) presents the schematic energy levels of the qubit-HO system with finite bias, where the left dashed lines are for the uncoupled and the right solid lines are for the coupled. Our dominant frequencies are related to the energy differences of the coupled qubit-HO system with numerical calculation. Parameters: $g = 0.18\Delta$, $\Gamma = 0.0154$, $\alpha=0.00493$.

Fig. 7 (color on the web) For off-resonance $\Delta = 0.5\Omega$ with larger qubit-HO coupling $g=0.7906\Omega$, (a) non-Markovian dynamics $P(t)$ and (b) its corresponding spectrum $S(\omega)$ at zero temperature is shown with bias $\epsilon = 0.1\Omega$ and with zero bias, while the Markovian ones in (a) has shown the long time limit. Similarly, the biased spectrum presents four dephasing peaks ($\omega_{10}, \omega_{20}, \omega_{21}, \omega_{30}$) and one relaxation peak ($\omega = 0$), while the unbiased one only presents two dephasing peaks. Insets: Inset (1) in (b) presents a magnification part. Inset (2) in (b) presents the schematic energy levels of the qubit-HO system with finite bias, where the left dashed lines are for the uncoupled and the right solid lines are for the coupled. Our dominant frequencies are related to the energy differences of the coupled qubit-HO system with numerical calculation. Parameters: $\alpha = 0.01$, $\Gamma = 0.002$.

Fig. 8 (color on the web) For near-resonance $\Delta = \Omega$ with larger qubit-HO coupling $g=0.7906\Omega$, (a) non-Markovian dynamics $P(t)$ and (b) its corresponding spectrum $S(\omega)$ at zero temperature is compared between the biased $\epsilon = 0.1\Omega$ and the unbiased at $\alpha = 0.05$, $\Gamma = 0.01$. Similarly, the biased spectrum presents four dephasing peaks (ω_{10} , ω_{20} , ω_{21} , ω_{30}) and one relaxation peak ($\omega = 0$), while the unbiased one only presents two dephasing peaks. Besides, with the same $\Delta = \Omega$, $g = 0.7906\Omega$ and $\epsilon = 0.1\Omega$, the effect with different Γ or α (red dot line: $\alpha = 0.01$, $\Gamma = 0.002$ and violet dash line: $\alpha = 0.1$, $\Gamma = 0.02$) is shown: the distributions of the dominant frequencies vary little, but with smaller Γ or α , the dephasing peaks will be higher and sharper and the dephasing will be smaller. Insets: Inset in (b) presents the schematic energy levels of the qubit-HO system with finite bias where the left dashed lines are for the uncoupled and the right solid lines are for the coupled. Our dominant frequencies are related to the energy differences of the coupled qubit-HO system with numerical calculation.

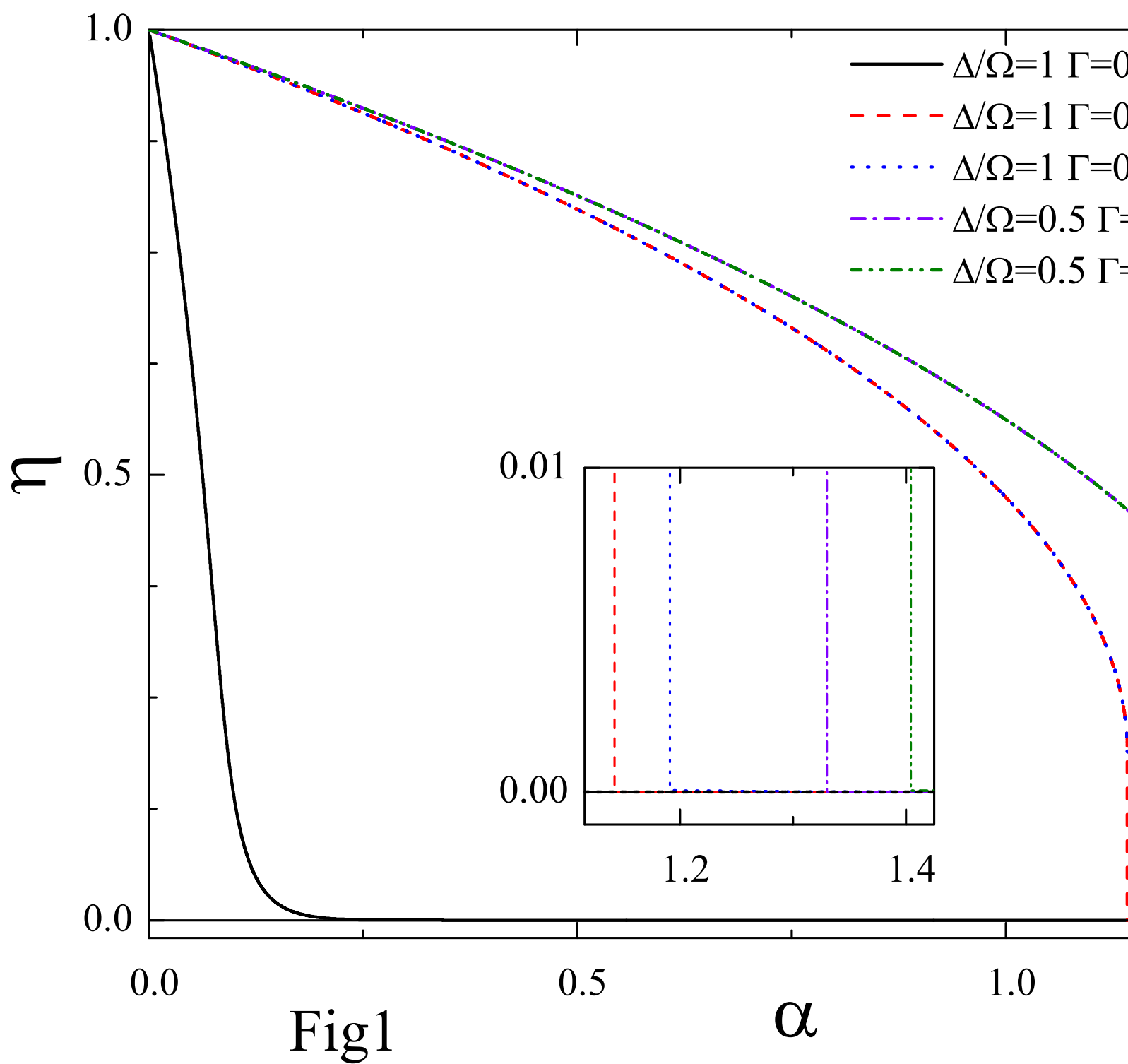
Fig. 9 (color on the web) Non-Markovian dynamics $P(t)$ for the near resonance case $\Delta = \Omega$ with $\epsilon = 0.1\Omega$ and $\Gamma = 0.01$ for different spin-bath coupling $\alpha = 0.005$, 0.05 , 0.1 , 0.2168 (corresponding qubit-HO coupling $g/\Omega = 0.25$, 0.7906 , 1.1180 , 1.6462) with all $\alpha < \alpha_c = 0.21683229$. It shows that when increasing α from weak to strong, the dynamics goes from abundant oscillation to nearly pure damping. Insets: The inset is the susceptibility $\chi''(\omega)$ vs. ω and it shows that when increasing α close to α_c the highest peak goes close to infinity near $\omega = 0$.

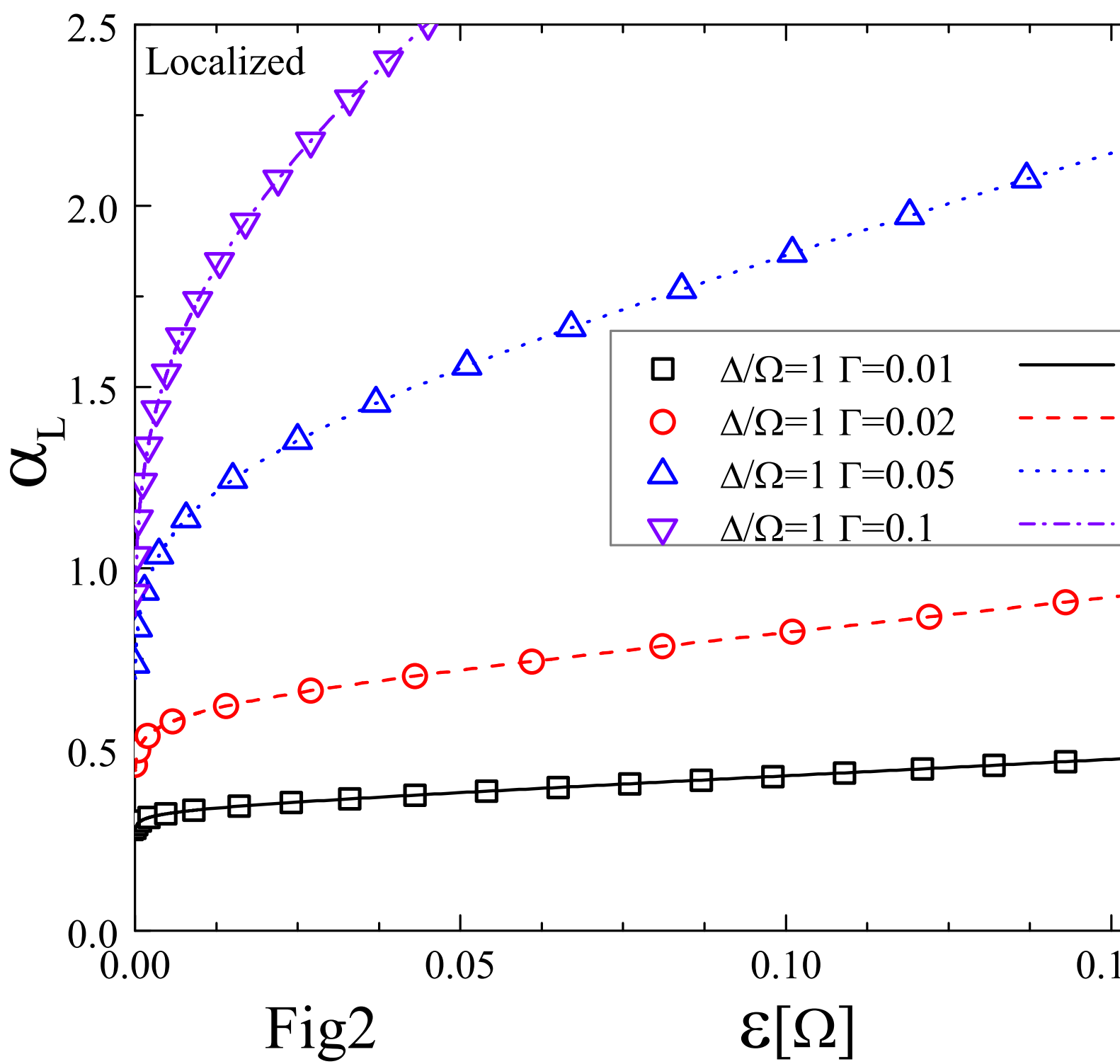
Fig. 10 Phase diagram of the coherent-incoherent transition point α_c vs. bias ϵ , for (a) near-resonance $\Delta = \Omega$ with different $\Gamma = 0.05$, 0.08 , 0.1 ; (b) off-resonance $\Delta = 0.5\Omega$ with different $\Gamma = 0.075$, 0.0762 , 0.08 , 0.1 . A kink appears when Γ is small for off-resonance, otherwise α_c gradually increases with ϵ .

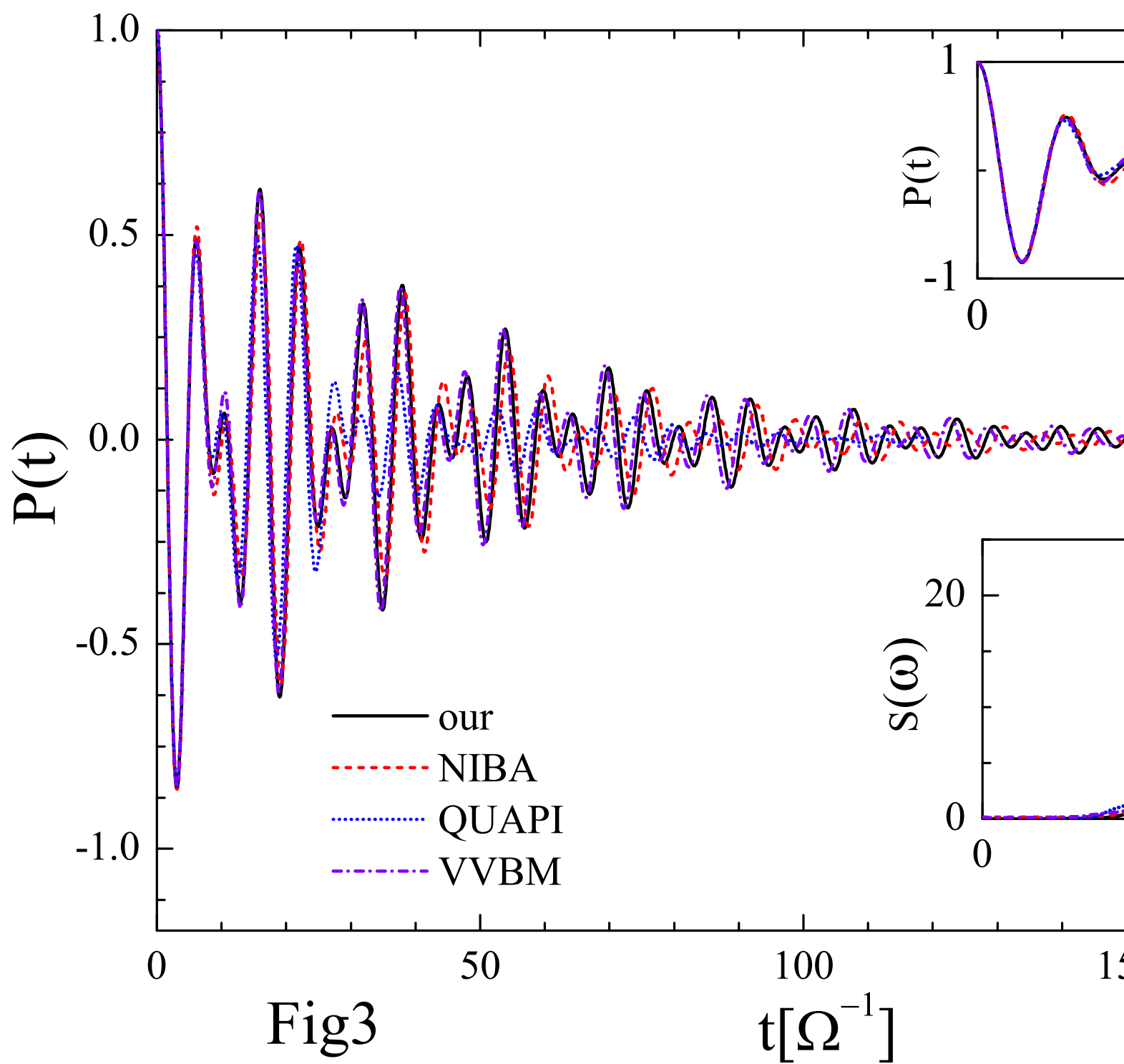
Tables

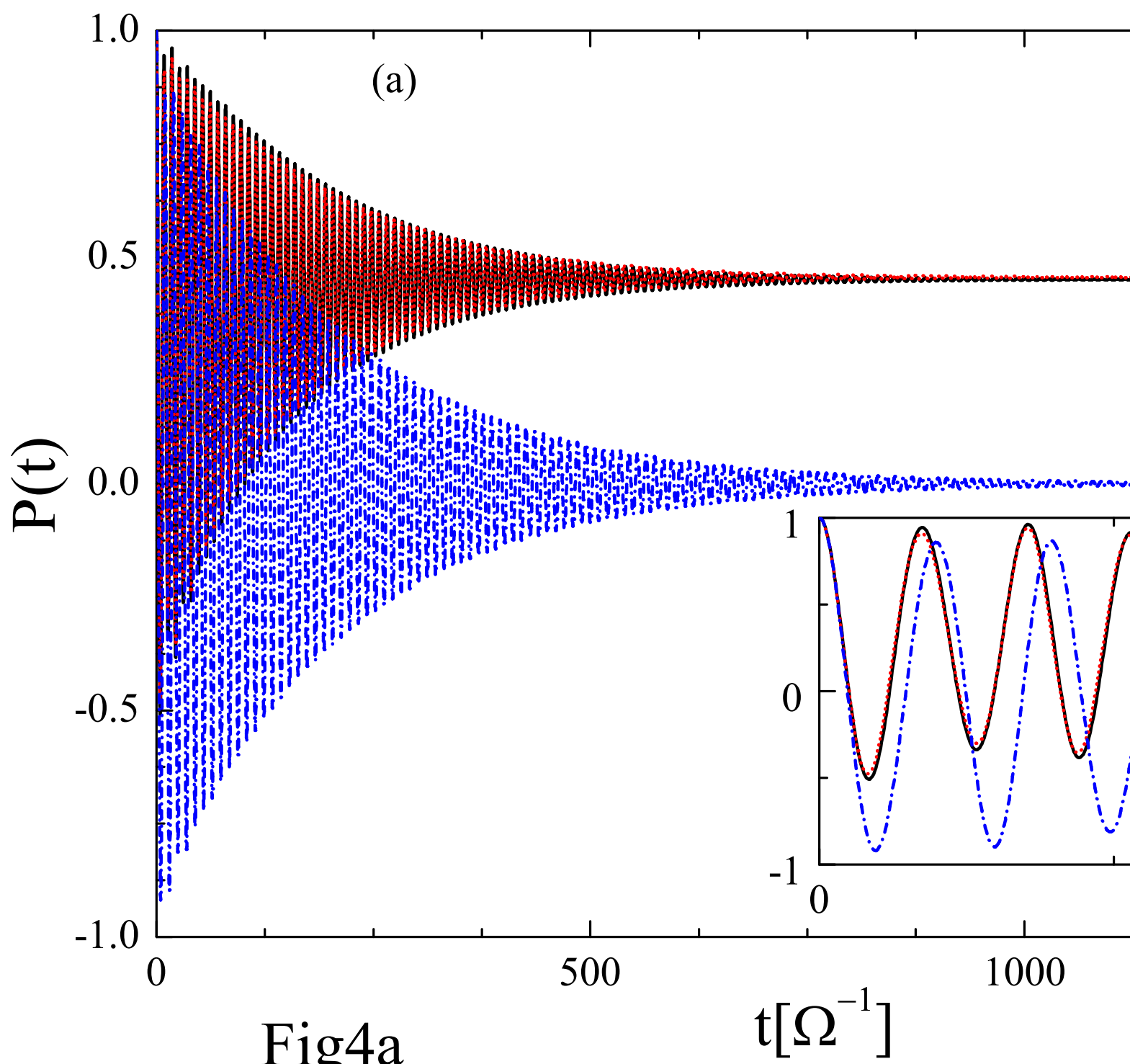
Table 1 The sum rule and the Shiba relation are checked with representative parameters. Here $R \equiv \lim_{\omega \rightarrow 0} F(\omega)/\frac{\pi}{4} [\chi'(0)]^2$, where $F(\omega) = \chi''(\omega)/J(\omega)$.

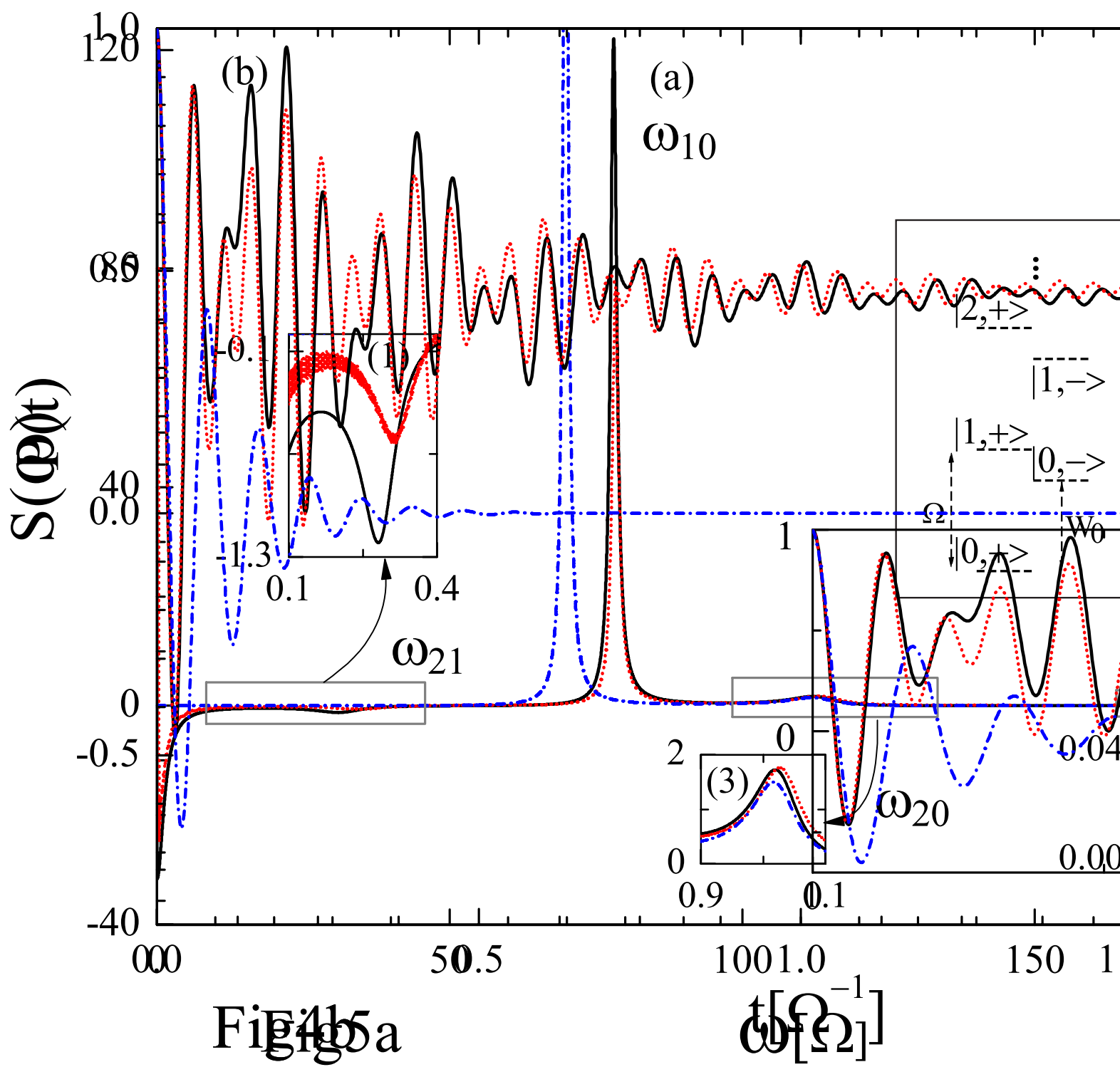
α	Δ/Ω	Γ	ϵ/Ω	$\chi'(0)$	$\lim_{\omega \rightarrow 0} F(\omega)$	R	$P(t=0)$
0.1	0.1	0.05	0.1	5.897376962	27.31540594	1	1
0.1	0.2	0.05	0.1	10.16150527	81.09722154	1	1
0.1	0.5	0.01	0	77.38519588	4703.332194	1	1
0.3	0.5	0.01	0.01	0.05845719399	0.002683896792	1	1
0.1	0.5	0.1	0.5	1.558179498	1.906886539	1	1
0.2	0.5	0.2	0.1	5.784656542	26.28119072	1	1
0.1	1	0.01	0	49.76240845	1944.879348	1	1
0.3	1	0.01	0.01	0.233784401	0.04292605141	1	1
0.1	1	0.01	0.1	36.23722191	1031.3348	1	1
0.21	1	0.01	0.1	7.819123532	48.01821704	0.9999999999	1
0.216	1	0.01	0.1	49.36762968	1914.143282	1.000000025	1
0.2168	1	0.01	0.1	1228.943521	1186131.33	0.9999517554	0.9999999947
0.2	1	0.05	0.01	7.857533292	48.49113404	1	1
0.5	1	0.2	0.1	5.312073901	22.1624668	1	1
0.1	1.1	0.05	0.1	2.920164619	6.697373981	1	1
0.2	1.2	0.01	0.1	7.494084145	44.10897966	1	1
0.1	1.5	0.05	0.1	2.003650314	3.15307092	1	1

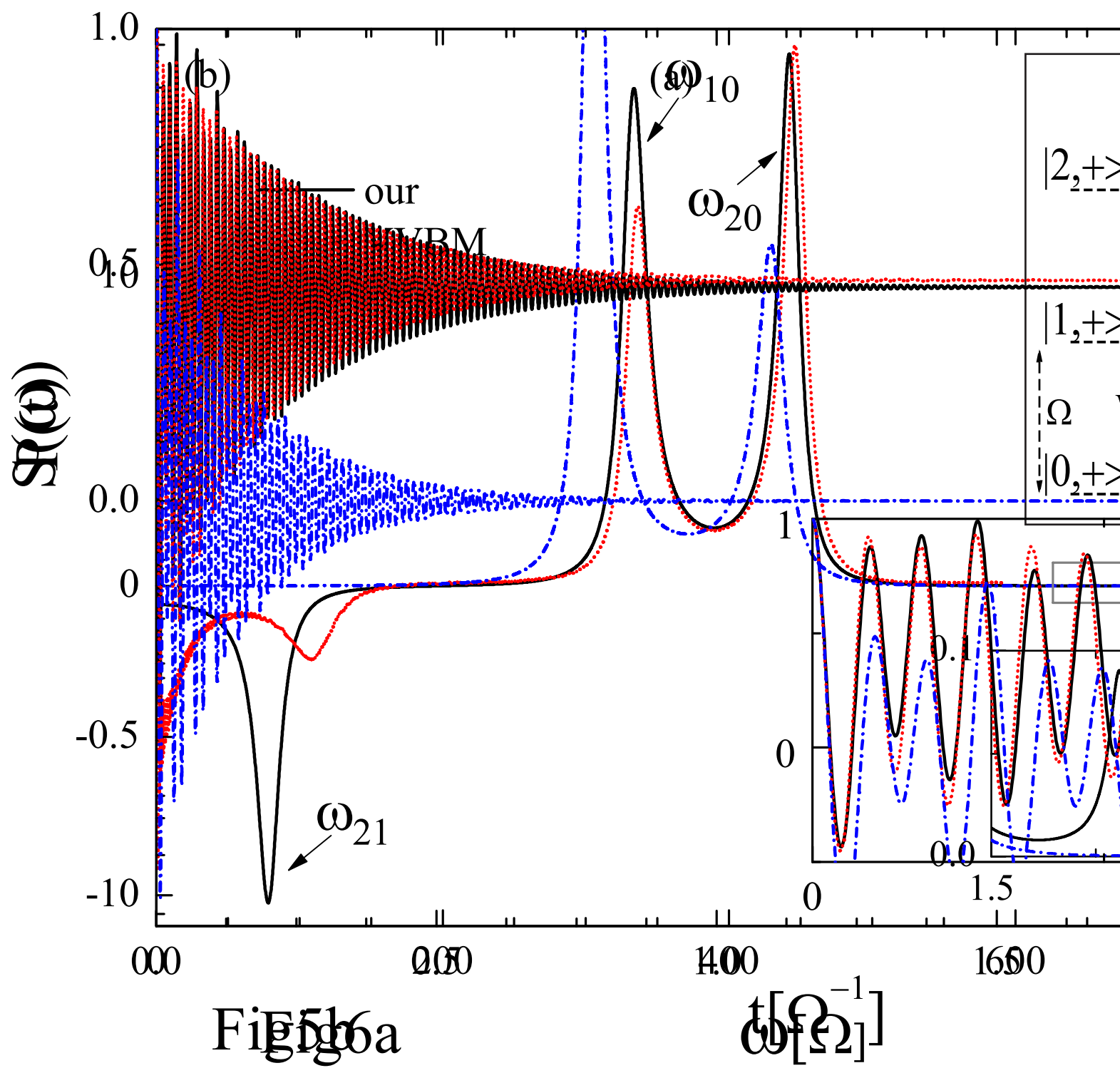


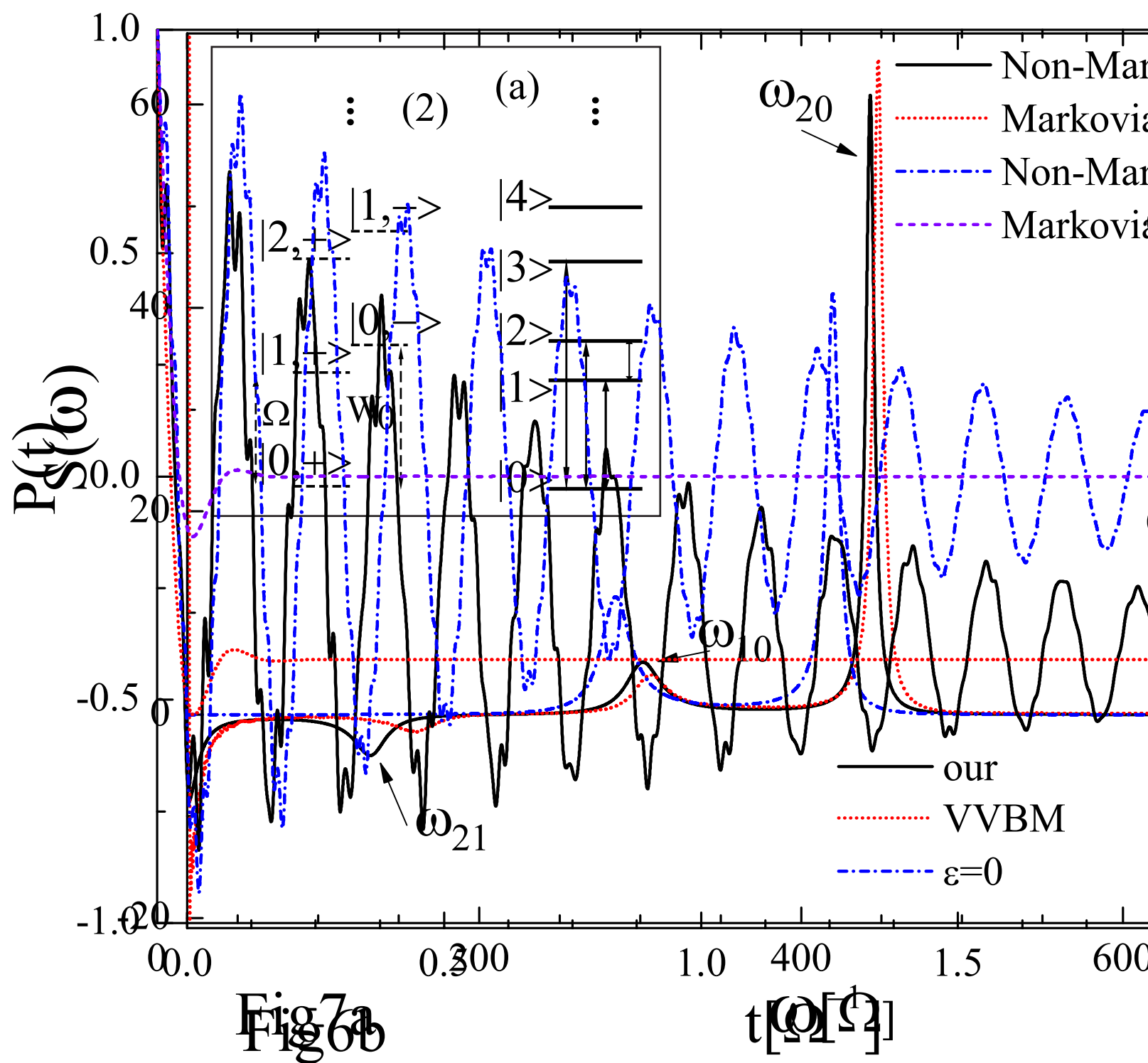


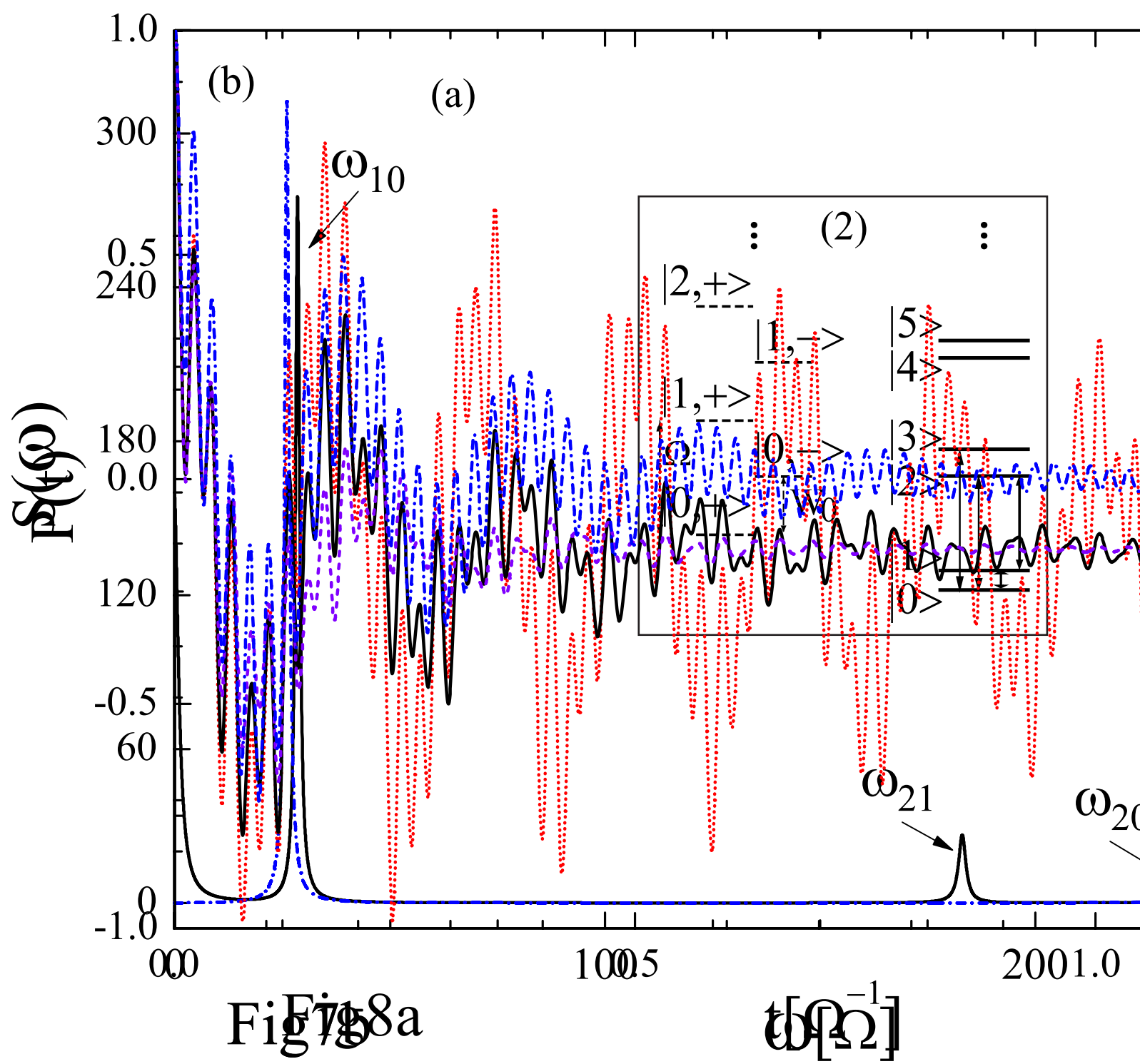


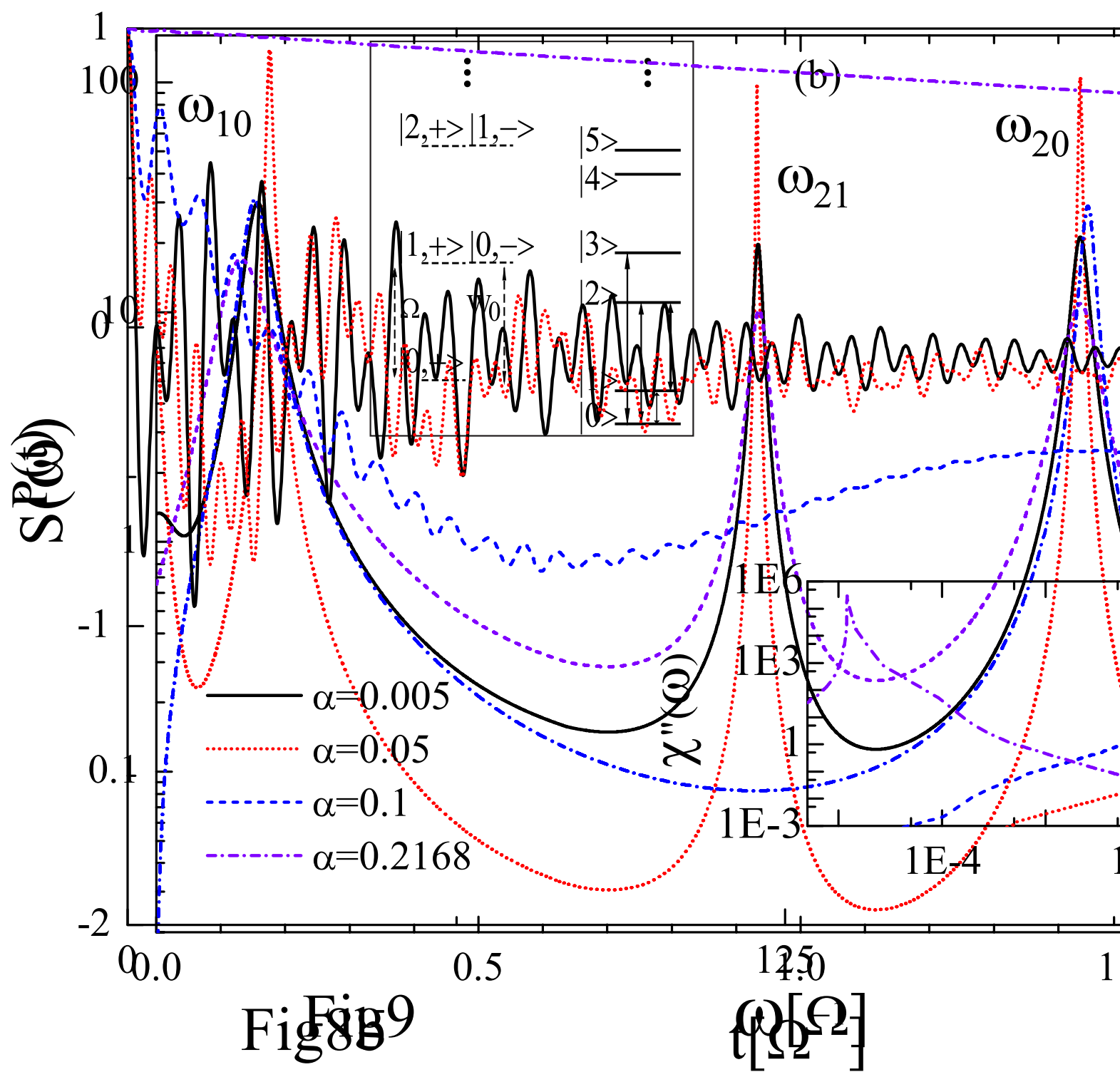


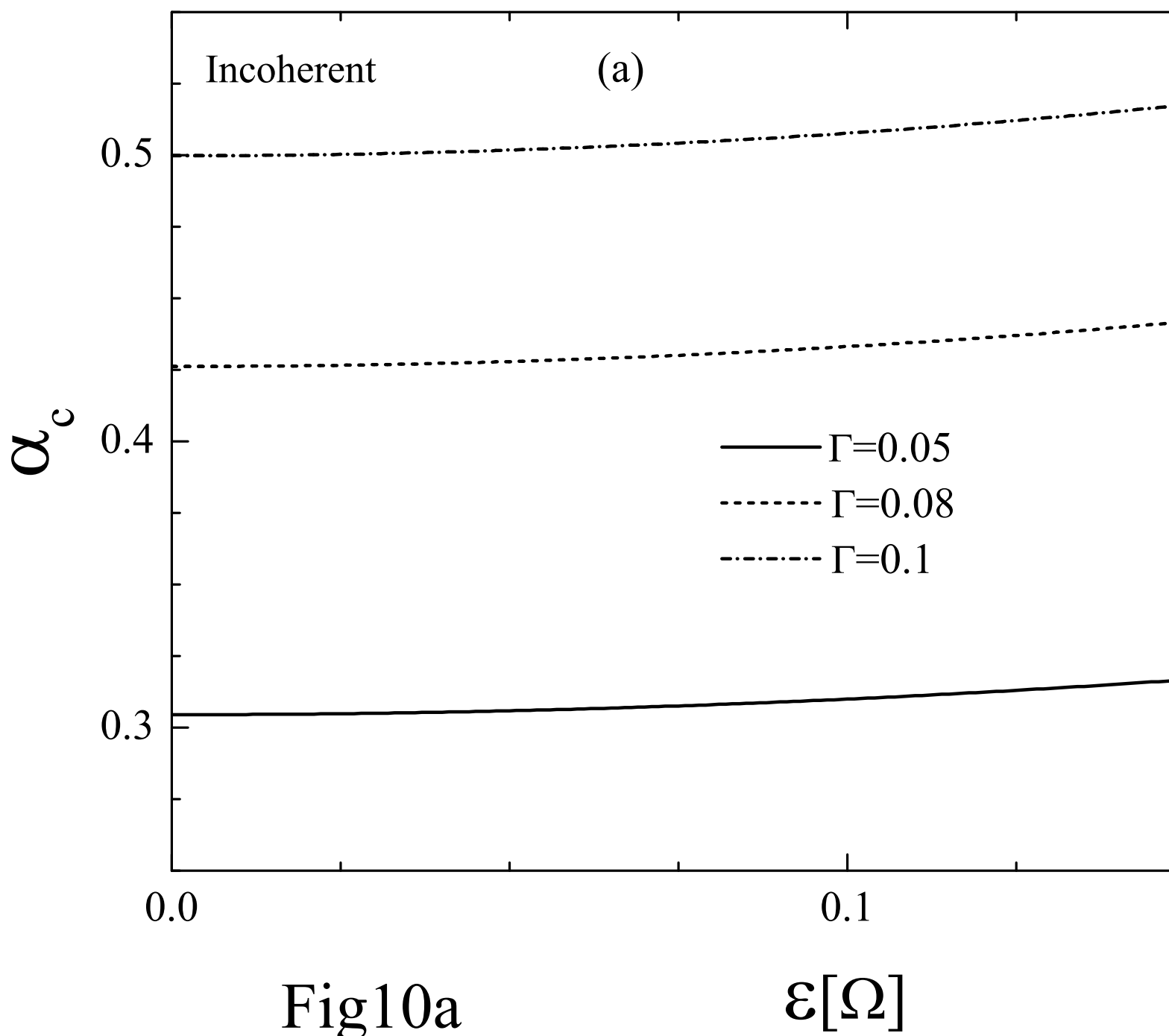












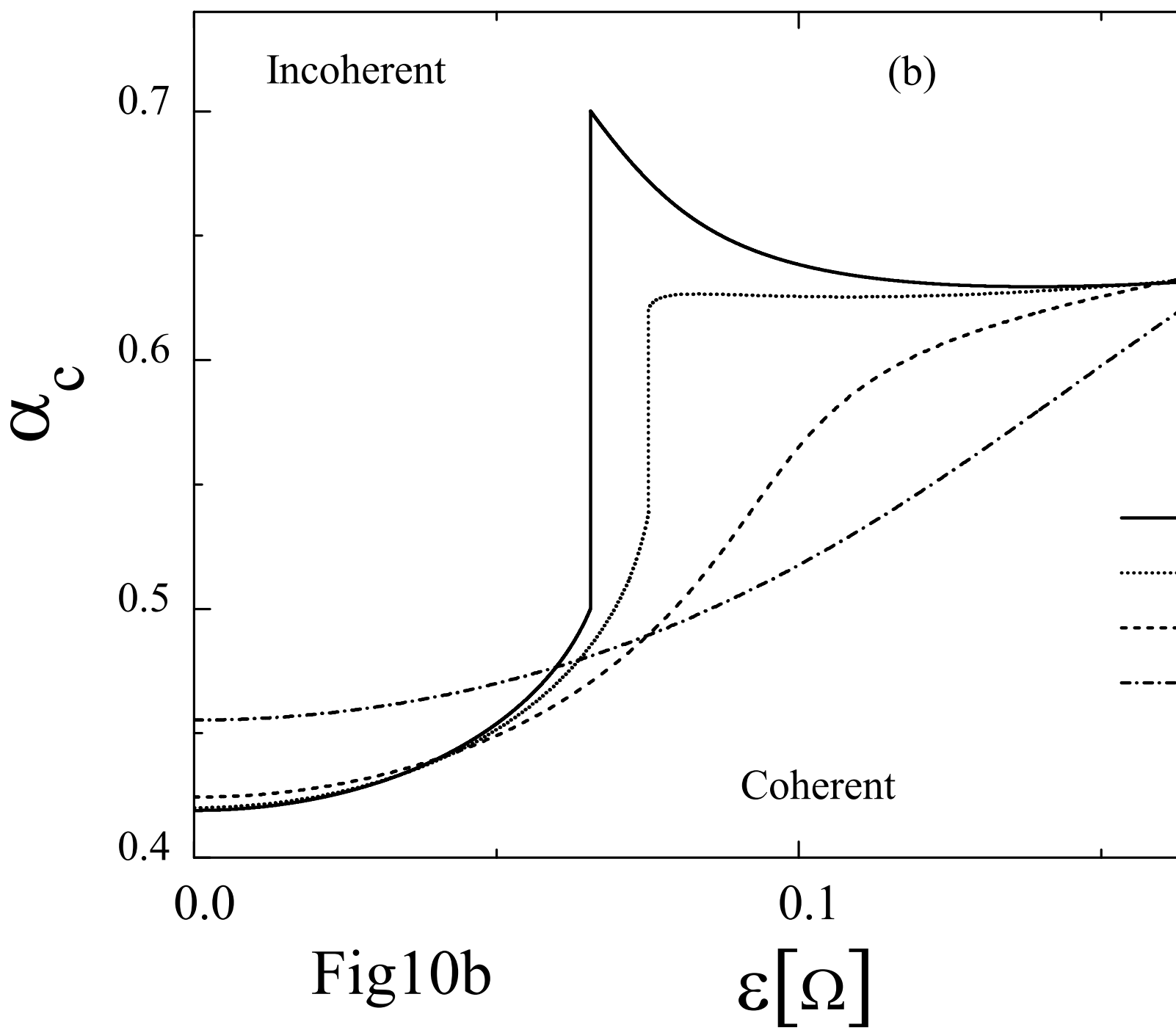


Fig10b